https://doi.org/10.5194/egusphere-2024-2085
Preprint. Discussion started: 2 August 2024

High metabolic zinc demand within native Amundsen and Ross Sea phytoplankton communities determined by stable isotope uptake rate measurements

Riss M. Kell[1,+], Rebecca J. Chmiel[1], Deepa Rao[1], Dawn M. Moran[1], Matthew R. McIlvin[1], Tristan J. Horner[1], Nicole L. Schanke[3], Robert B. Dunbar[2], Giacomo R. DiTullio[3], Mak A. Saito[1]

[1]Department of Marine Chemistry and Geochemistry, Woods Hole Oceanographic Institution, Woods Hole, MA, USA

[2]Doerr School of Sustainability, Stanford University, Stanford, CA 94305

[3]Hollings Marine Laboratory, College of Charleston, Charleston, South Carolina, 29412, USA

Correspondence to: Mak A. Saito (msaito@whoi.edu)

[+]Formerly published under Riss Kellogg; now affiliated with Gloucester Marine Genomics Institute, Gloucester MA, 01930-3006

Abstract

Zinc (Zn) is an essential micronutrient for most eukaryotic phytoplankton. Zn uptake by phytoplankton within the euphotic zone results in nutrient-like dissolved Zn profiles (dZn) with a large dynamic range. The combination of key biochemical uses for Zn and large vertical gradients in dZn implies the potential for rapid rates of Zn removal from the surface ocean. However, due to the ease of contamination at sea, direct measurements of dZn uptake within natural environments have not been previously made. To investigate the demand for dZn and for dissolved cadmium (dCd; a closely related nutrient-like element) within Southern Ocean phytoplankton communities, we conducted ^{67}Zn and ^{110}Cd tracer uptake experiments within the Amundsen Sea, Ross Sea, and Terra Nova Bay into the >3 μm phytoplankton particulate size fraction. The highly productive Amundsen Sea and Ross Sea of Antarctica host large phytoplankton blooms in the austral spring and summer, during which macronutrient and

https://doi.org/10.5194/egusphere-2024-2085
Preprint. Discussion started: 2 August 2024

micronutrient surface concentrations become significantly depleted largely due to phytoplankton uptake. In autumn and winter, nutrient levels are "reset" to high concentrations throughout the water column in these environments due to convective overturn, advancing sea ice cover, and darkness. This annual "resetting" of nutrient concentrations makes these Antarctic environments ideal locations to study the seasonal demand for Zn within these productive communities.

In this study, variations in metal uptake rates over depth and time and correlations with other oceanic parameters were examined. High total metal uptake rates (ρMetal) of both Zn and Cd were consistent with the observed depletion of dZn and dCd surface concentrations. Our findings suggest that high biomass and low seawater pCO_2 exerted primary control over increasing ρZn, which in turn led to increases in ρCd likely through the upregulation of shared transport systems. Overall, we observed a high magnitude of Zn uptake (> 100 pmol dZn L^{-1} d^{-1}) into the particulate phase within these Southern Ocean phytoplankton communities, suggesting that even in the Zn-rich waters of the Southern Ocean, high Zn uptake rates can lead to Zn depletion and potential Zn scarcity.

1 Introduction

Zinc (Zn) is an essential trace metal micronutrient for marine phytoplankton with roles in carbon fixation, organic phosphorus uptake, and transcriptional and translational processes, among others (Shaked et al. 2006; Morel et al. 2013, 2020; Twining and Baines 2013). Nutrient-like depth profiles of total dissolved Zn (dZn) are characterized by depleted surface concentrations due to uptake by phytoplankton within the euphotic zone, reflecting this high biological demand (Fitzwater et al. 2000; Lohan et al. 2002; Zhao et al. 2014; Middag et al. 2019). Zn is particularly important as a catalytic cofactor in carbonic anhydrase (CA) metalloenzymes, which catalyze the reversible dehydration of HCO_3^- to CO_2. As HCO_3^-

https://doi.org/10.5194/egusphere-2024-2085
Preprint. Discussion started: 2 August 2024

constitutes about 90% of the dissolved inorganic carbon (DIC) pool in the surface ocean, CAs in marine algae are a critical part of the carbon concentrating mechanism (CCM) that maintains a CO_2 supply to the carbon-fixing enzyme ribulose-1,5-biphosphate carboxylase/oxygenase (RUBISCO). Less abundant divalent metal cations such as cobalt (Co^{2+}) and cadmium (Cd^{2+}) can replace Zn^{2+} in some algal CA subtypes (Lane et al. 2005), conferring biochemical flexibility to algae confronted with low Zn bioavailability.

While Cd is known to cause toxic effects in most organisms (Brand et al. 1986; Das et al. 1997), dCd depth profiles are also nutrient-like. As noted above, the biological use of Cd as a catalytic cofactor within Cd-containing carbonic anhydrase (ζ-CA, or CDCA) likely contributes to surface dCd depletion and thus to the observed nutrient-like profiles, though this remains the only known biological use of Cd to date (Lee and Morel 1995; Sunda and Huntsman 2000; Haas et al. 2009). It has also been proposed that phytoplankton may assimilate Cd abiotically—this mode of Cd uptake is non-specific, a case of 'mistaken identity' in which phytoplankton bind and store imported Cd inside the cell to avoid toxicity, coupling the cycling of Cd to the biological cycle of nutrients (Horner et al. 2013). As the beneficial effect of adding Cd to phytoplankton cultures has only been observed when Zn is limiting (Price and Morel 1990; Lee et al. 1995; Xu et al. 2007), it has been speculated that the ability to use Cd in place of Zn in CDCA may confer a competitive advantage to Zn-limited algae under low pCO_2. To date, homolog *cdca* genes have been found exclusively in diatom species (Park et al. 2007, 2008). However, since the beneficial effect of Cd has also been observed in organisms such as the green alga *Tetraselmis maculata* and the coccolithophore *Emiliania huxleyi* that lack the *cdca* gene (Lee and Morel 1995), it is thought that Cd may have other biochemical functions in phytoplankton still awaiting discovery.

https://doi.org/10.5194/egusphere-2024-2085
Preprint. Discussion started: 2 August 2024

Globally, dZn concentrations share a near-linear correlation with those of dissolved silicate (Bruland et al. 1978), a macronutrient required by diatoms to form their siliceous frustules. While this would seem to suggest that Zn is predominantly present in and remineralized simultaneously with siliceous diatom frustules at depth, this is not the case. Only a small fraction of cellular Zn (1-3%) is incorporated into frustules (Ellwood and Hunter 2000) while the majority of Zn is instead associated with diatom organic matter (Twining et al. 2004). Furthermore, cellular Zn within sinking diatom detritus is remineralized over the same short length-scale as phosphorus (P) as opposed to the greater depths at which siliceous material remineralizes (Twining et al. 2014).

Hypotheses to explain the coupling of Zn and Si generally propose that a combination of physical and biogeochemical processes (including reversible adsorption of Zn onto sinking organic particles (Weber et al. 2018)) give rise to the Zn:Si relationship, with strong Zn drawdown by Southern Ocean diatoms and the resulting export of Zn-rich biogenic particles acting as a key influence (Vance et al. 2017). This is complemented by the observation that Southern Ocean diatom species possess cellular Zn quotas that are 3-15x higher compared to those of low-latitude species (Twining and Baines 2013), and Zn is rapidly stripped from Southern Ocean surface waters (Ellwood 2008; Zhao et al. 2014). This rapid removal of Zn may be, in part, due to low seawater pCO_2 resulting from bloom conditions during austral summer that further exacerbates the need for inorganic carbon acquisition by photosynthetic phytoplankton, which in turn exacerbates Zn demand through its use as a cofactor in carbonic anhydrase (Kell et al. 2023). Ocean biogeochemical modeling studies have demonstrated that model variants with high (> 4.5 mmol:mol) Zn:P uptake ratios are able to reproduce the Zn-Si correlation without any explicit coupling between Zn and Si (Vance et al. 2017; de Souza et al.

https://doi.org/10.5194/egusphere-2024-2085
Preprint. Discussion started: 2 August 2024

2018; Roshan et al. 2018), suggesting that rapid Zn removal into the particulate phase is a key feature of biogeochemical cycling in the Southern Ocean.

The rapid removal of dZn from the surface within the Southern Ocean suggests the possibility for phytoplankton growth to become Zn-limited. While phytoplankton growth in the Southern Ocean is well-known to be primarily limited by Fe availability (Martin 1990; Arrigo et al. 2008), melting icebergs and ice shelves are known to act as external sources of Fe (St-Laurent et al. 2017; Hopwood et al. 2019; Person et al. 2021) with larger Fe inputs expected from increased ice melt in a warming climate. Increased dFe inputs to surface Antarctic waters may act to relieve Fe stress, but would simultaneously support the development of other nutrient limitations. For example, low availabilities of both dZn and vitamin B_{12} have been previously observed to co-limit phytoplankton growth with Fe in the Ross Sea (Bertrand et al. 2007; Kell et al. 2023). A high demand for Zn naturally exists within eukaryotic phytoplankton due to the requirement for Zn^{2+} in numerous metabolic functions— therefore, without similarly enhanced inputs of dZn to the water column, the alleviation of primary Fe limitation could induce Zn stress as the next most in-demand metal micronutrient. Coastal polynyas that form within the Amundsen and Ross Seas during austral spring and summer are particularly primed to experience Zn stress as these regions host highly productive seasonal phytoplankton blooms that act as significant carbon sinks (Arrigo et al. 2012). This high productivity draws pCO_2 down to low levels (< 200 ppm), putting pressure on the carbon concentrating mechanism of photosynthetic phytoplankton to acquire CO_2 and thus to acquire Zn as the predominantly utilized metal cofactor within carbonic anhydrases.

The present study enhances our knowledge of what constitutes the anticipated high levels of Zn uptake in the Southern Ocean with empirical field data measured within native Southern

https://doi.org/10.5194/egusphere-2024-2085
Preprint. Discussion started: 2 August 2024

Ocean phytoplankton communities. This study developed a field-based, stable Zn isotope uptake rate method, building on a prior stable Cd uptake rate method (Cox et al. 2014). While Zn uptake has been measured in laboratory cultures (Sunda and Huntsman 1992, 1995, 2000), and the influence of grazing and tropic transfer studies have been conducted using radioactive isotopes (Hutchins and Bruland 1994, 1995), to our knowledge direct measurements of Zn uptake in natural marine phytoplankton communities have not been conducted previously, despite interest in modeling its biogeochemical uptake and cycling (Weber et al. 2018). We measured the total uptake rates of Zn and Cd along the shelves of the Amundsen Sea and Ross Sea during the austral summer of 2017-2018 (December – March). This was accomplished by introducing ^{67}Zn and ^{110}Cd (with natural abundances of 4.10% and 12.5%, respectively) into short-term (24 hr) incubation experiments. The aim was to quantify the transfer of dissolved $^{110}Cd^{2+}$ and $^{67}Zn^{2+}$ into the particulate fraction exceeding 3 µm. Both stable isotopes can be used as uptake tracers by analysis of isotope abundances that deviate from natural abundances within the particulate phase. The transfer of added isotopes into the particulate phase is the combined result of 1) active transport of metal into cells, 2) nonspecific metal adsorption to cell surfaces, 3) metal adsorption to non-living particulate organic matter, and 4) metal adsorption to particulate inorganic matter, though we expect active transport into cells to dominate the measured particulate isotopic signal due to the high abundance of actively growing autotrophic cells in the photic zone observed in the Southern Ocean during austral summer. These measurements of uptake rates were then used to infer timescales of surface dZn and dCd depletion in these Antarctic environments. These uptake rates contribute to understanding the biological demand and potential for Zn limitation of primary productivity in highly productive coastal environments, such as the polynyas surrounding Antarctica (Kell et al. 2023).

https://doi.org/10.5194/egusphere-2024-2085
Preprint. Discussion started: 2 August 2024

2 Materials and methods

2.1 Study area and sample collection

Samples were collected during the CICLOPS (Cobalamin and Iron Co-Limitation of Phytoplankton Species) expedition (NBP18-01) aboard the RVIB *Nathaniel B. Palmer*, December 11, 2017 – March 3, 2018 in the Amundsen Sea and Ross Sea of the Southern Ocean (**Fig. 1**).

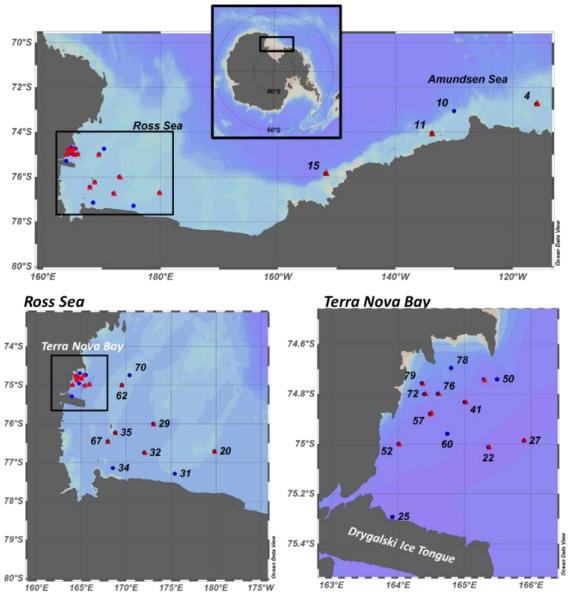

Figure 1. Map showing the stations sampled over the course of the CICLOPS cruise. Stations marked by red triangles indicate those at which stable 67Zn and 110Cd uptake rate experiments were performed. An expanded map of stations sampled in the Ross Sea is shown at bottom left, while a further expansion of stations sampled in Terra Nova Bay is shown at bottom right.

Station metadata is given in **Table S1**. Water samples were collected using trace metal clean (TMC) sampling protocols described previously (Cutter and Bruland 2012). A TMC rosette suspended on a Kevlar line and equipped with twelve 8L X-Niskin bottles (Ocean Test Equipment) was used to collect seawater at depths ranging from 10 – 600 m. Continuous

https://doi.org/10.5194/egusphere-2024-2085
Preprint. Discussion started: 2 August 2024

underway measurements of pCO_2 measurements at ~5 m depth were taken using a pCO_2 measurement system from Lamont-Doherty Earth Observatory (LDEO, 0.017/sec rate). Hydrography data were collected using sensors deployed on a titanium trace metal rosette (TMR) in tandem with TMC niskin bottles. The TMR was equipped with sensors to measure temperature, conductivity, pressure, dissolved oxygen, chlorophyll (Chl) fluorescence, altimetry, beam transmission, and photosynthetically active irradiance (PAR). Chl fluorescence was measured using a WetLabs ECO-FL fluorometer. A complete data report and sensor list are available at NBP1801DATA.pdf (rvdata.us). Mixed layer depth (MLD) was determined for each station within Terra Nova Bay as the first depth at which the difference between the potential density (σ_θ) and reference density (the potential density at 10m, σ_{ref}) was greater than or equal to 0.125 kg m^{-3} (Bishop and Wood 2009; Ohnemus et al. 2017).

2.2 Preparation of plasticware

Polyethylene and polycarbonate sampling and incubation bottles were rigorously cleaned to remove trace metal contaminants before use. Bottles with rinsed with Milli-Q water (Millipore), soaked for 72h in <1% Citranox detergent, rotated, soaked for an additional 72h, and then rinsed five times with Milli-Q water. Bottles were then filled with 10% HCl (Baker instra-analyzed) by volume and soaked for a minimum of one week, rotated, and soaked for another week. Bottles were then rinsed five times with dilute acid (HCl, pH 2) and stored double-bagged in plastic zip bags. All cleaning work was conducted in a Class 100 clean room.

2.3 Analyses of total dissolved Cd and Zn using isotope dilution

Samples for the analysis of total dissolved Zn, Cd, Fe, Mn, Cu and Ni concentrations were collected shipboard by pressure-filtering X-Niskin bottles through an acid-washed 142mm, 0.2µM Supor membrane filter (Pall) within 3 hours of rosette recovery using high purity

https://doi.org/10.5194/egusphere-2024-2085
Preprint. Discussion started: 2 August 2024

(99.999%) N_2 gas. Total dissolved water samples were collected into 250 mL TMC polyethylene bottles and were stored double-bagged in plastic zip bags. Seawater samples for ^{110}Cd and ^{67}Zn stable isotope uptake experiments were collected in the same way but without filtering. All sample collection occurred shipboard within a TMC van containing laminar flow hoods and plastic sheeting. Samples for total dissolved metal analysis were acidified to pH 1.7 with high purity HCl (Optima, Fisher Scientific) within 7 months of sampling and were stored acidified at room temperature for over 1 year prior to analysis.

Quantification of dissolved metals in samples and reference seawater was performed for total dissolved Fe, Ni, Cu, Zn, and Cd using isotope dilution. 15 mL of acidified seawater sample was spiked with 50 µL of a stable isotope spike solution artificially enriched in ^{57}Fe, ^{61}Ni, ^{65}Cu, ^{67}Zn, and ^{110}Cd. All stable isotopes were received in solid form (Oak Ridge National Laboratory). Initial dissolution and all subsequent dilutions were made using concentrated nitric acid (Optima, Fisher Scientific). Concentrations and ratios of isotopes for each metal in the spike solution were verified by inductively coupled plasma mass spectrometry (ICP-MS) using a multi-element standard curve (SPEX CertiPrep). The composition of the isotope spike addition was made such that the target isotope ratios in the total, 15mL spiked sample would be $^{57}Fe/^{56}Fe$ = 0.7, $^{61}Ni/^{60}Ni$ = 0.5, $^{65}Cu/^{63}Cu$ = 1, $^{67}Zn/^{66}Zn$ = 0.7, and $^{110}Cd/^{114}Cd$ = 1 and were verified with ICP-MS. These ratios were chosen to minimize the uncertainty introduced by error propagation through the isotope dilution equation (Wu and Boyle 1998; Rudge et al. 2009; Tan et al. 2020). The same spike solution was used to spike all samples from all depths. Because it is monoisotopic, total dissolved Mn was calculated using a modified isotope dilution equation:

$$\text{Mn (nM)} = \frac{^{55}\text{Mn}_{\text{spl}}\,(\text{cps})}{^{57}\text{Fe}_{\text{spl}}\,(\text{cps})} * {}^{57}\text{Fe}_{\text{spike}}\ (\text{nM}) * {}^{57}\text{Fe}_{\text{slope}}\ (\text{cps/ppb}) * \frac{1}{(^{55}\text{Mn}_{\text{slope}})\ (\text{cps/ppb})} \quad (1)$$

https://doi.org/10.5194/egusphere-2024-2085
Preprint. Discussion started: 2 August 2024

in which $^{55}Mn_{spl}$ and $^{57}Fe_{spl}$ refer to the blank corrected counts per second (cps) of ^{55}Mn and ^{57}Fe in the spiked sample, ^{57}Fe spike is the concentration of ^{57}Fe spike, $^{57}Fe_{slope}$ is the slope of the external standard calibration curve (SPEX curve) relating ^{57}Fe cps to ppb, and $^{55}Mn_{slope}$ is the slope of the external calibration curve (SPEX curve) relating ^{55}Mn cps to ppb. Due to the acidification of seawater prior to ICP-MS analysis, Mn ICP-MS measurements do not include contributions from humic-type Mn(III)-ligand complexes (Oldham et al. 2021). Until the inclusion of Mn(III) is resolved and intercalibrated, we report these Mn values as Mn(II) and note that they are consistent with prior studies employing the same acidification technique (Sedwick et al. 2000; Noble et al. 2013; Gerringa et al. 2020).

Preconcentration of spiked seawater samples for total dissolved metal analysis was performed using the automated solid phase extraction system seaFAST-pico (Elemental Scientific) in offline concentration mode with an initial volume of 15 mL and elution volume of 500 µL (Bown et al. 2017; Rapp et al. 2017; Jackson et al. 2018; Wuttig et al. 2019). The seaFAST contains a Nobias-chelate PA1 resin column (ethylenediaminetriacete and iminodiacetate) suitable for the simultaneous preconcentration of several trace metals (Fe, Mn, Zn, Cu, Co, Cd, Ni) with high sensitivity and quantitative recovery (Sohrin et al. 2008; Biller and Bruland 2012). Adjusted seaFAST software settings were a 17 second load loop time and a single 10 mL load cycle. Process blanks consisted of pH 2 HCl (Optima, Fisher Scientific) and were processed as samples to account for any contamination introduced by instrument processing.

Reagents consisted of a 1.5M ammonium acetate pH 6.0 buffer made using glacial acetic acid and ammonium hydroxide (20-22%) of the highest purity (Optima, Fisher Chemical), a 1% nitric acid rinse solution (Optima grade, Fisher Chemical), and a 10% nitric acid elution buffer

https://doi.org/10.5194/egusphere-2024-2085
Preprint. Discussion started: 2 August 2024

(Optima grade, Fisher Chemical) with 10 ppb indium (^{115}In, SPEX CertiPrep) added as an internal standard. Solutions were prepared with 18.2 Ω Milli-Q water (Millipore). Polypropylene 15 mL centrifuge tubes used in sample processing were cleaned of potential metal contamination by soaking in 10% HCl for 5 days and rinsing with pH 2 HCl prior to use.

Following offline seaFAST preconcentration, multi-elemental quantitative analysis was performed using an iCAP-Q inductively coupled plasma-mass spectrometer (Thermo Scientific). To minimize oxide interference on metal isotopes, a cooled spray chamber and helium collision gas were employed. Analytes were measured in single quadruple mode (kinetic energy discrimination [KED]). Concentrations of Mn, Fe, Ni, Cu, Zn and Cd were determined using a six-point external standard curve of a multi-element standard (SPEX CertiPrep), diluted to range from 1-10 ppb in 5% nitric acid. An indium standard (SPEX CertiPrep) was similarly added to these standard stocks, diluted to range 1-10 ppb. Instrument injection blanks consisted of 5% nitric acid in Milli-Q. Standard curve R^2 values were ≥ 0.98 for all metals monitored. Method accuracy and precision were assessed using the 2009 GEOTRACES coastal surface seawater (GSC) standard (n = 8; **Table S3**), which produced values consistent with consensus results.

2.4 Uptake experiments: ^{67}Zn and ^{110}Cd spiking, incubation, and sample collection

^{67}Zn and ^{110}Cd and stable isotope uptake experiments were modeled after those conducted by Cox et. al. 2014, with the addition of Zn uptake measurements. An overall schematic detailing these experiment workflows is shown in **Fig. 2**.

https://doi.org/10.5194/egusphere-2024-2085
Preprint. Discussion started: 2 August 2024

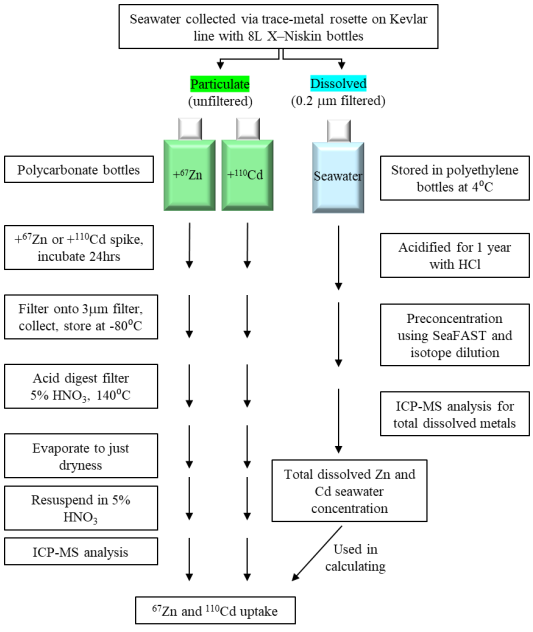

Figure 2. Diagram showing the overall workflow used to measure particulate uptake of ^{110}Cd and ^{67}Zn and total dissolved Cd and Zn, after Cox et al. 2014.

Uptake experiments were performed at 18 stations total (**Fig. 1**). Raw (unfiltered) seawater was collected shipboard over a depth range of 10 – 600 m into 250 mL TMC polycarbonate incubation bottles. All incubation bottles were filled with minimal headspace such that the total culture volume was ~275 mL. Two incubation bottles per depth were filled with raw seawater— one was spiked with ^{67}Zn, the other was spiked with ^{110}Cd. The Cd and Zn isotope spikes were prepared by dissolving ^{110}CdO and ^{67}ZnO (Oak Ridge National Laboratory) in 5% HNO_3 (Seastar Baseline) and were diluted using Milli-Q water to minimize added acidity. When added to the filled incubation bottles, the total added (spiked) concentration of Cd was 300 pM and the total added concentration of Zn was 2 nM. The chosen total added concentrations were based on the surface ratio of total dissolved Cd (dCd) to total dissolved Zn (dZn) reported previously for the Ross Sea (Fitzwater et al. 2000). Immediately after spiking, incubation bottles

https://doi.org/10.5194/egusphere-2024-2085
Preprint. Discussion started: 2 August 2024

were sealed, inverted to mix, and transferred to flow-through on-deck incubators for 24hr. Incubators were shielded by black net neutral density screening to allow 20% ambient light penetration.

Biomass was collected after 24hr by vacuum filtering the entire volume of each incubation sample at 34.5 kPa (5 psi) onto an acid-cleaned 3μm, 50mm acrylic copolymer (Versapore) filter (Pall) mounted on an acid-cleaned Teflon (Savillex) filtration rig. Samples were filtered through 3 μm pore-size filters rather than 0.2 μm in order to minimize filtration time (and thus time exposed to potential contamination) and to capture the bulk of eukaryotic phytoplankton biomass typically found in the Southern Ocean. An aliquot of 1 mL of 0.2 μm filtered surface seawater (collected at 10 m depth) was used to rinse the sample before collecting the filter into an acid-cleaned 2 mL cryovial using acid-rinsed plastic forceps. Filter blanks were duplicate 3 μm acid-clean Versapore (Pall) filters that were placed onto the filtration rig, rinsed with filtered surface seawater, collected, stored, and processed as samples were to correct for any contaminating metals present on the filters themselves. Blanks were collected at each station. Filters were stored frozen at -80 ºC in acid-cleaned cryovials until analysis. The filtration rig was rinsed with pH 2 HCl between samples. Polycarbonate incubation bottles were cleaned between stations with a 10% HCl rinse and several rinses in Milli-Q water, followed by a brief soak in 10% HCl followed by a pH 2 HCl rinse. All spike addition and sample filtration procedures were completed in a fabricated shipboard positive-pressure clean room environment made of laminar flow hoods and plastic sheeting.

We note that the total Zn and Cd uptake rate values presented in this study represent potential uptake rates rather than true uptake rates—this naturally arises as a consequence of adding the spiked tracer ^{67}Zn and ^{110}Cd into raw surface seawater. As this seawater is naturally

https://doi.org/10.5194/egusphere-2024-2085
Preprint. Discussion started: 2 August 2024

depleted in both metals, the spike addition artificially increases the total Zn and Cd present and thus could perturb the response of biology to these additions. It should also be noted that both ^{67}Zn and ^{110}Cd spikes were not equilibrated with natural seawater before their addition to incubation bottles to maintain experimental consistency. Experiments of this nature have been conducted previously using radioisotopes as tracers (Morel et al. 1994; Sunda and Huntsman 1995; Cullen et al. 1999; Hutchins et al. 1999), though we chose to use stable isotopes for ease of shipboard use and waste disposal.

2.5 Filter digestion and particulate ICP-MS analysis

All work was performed in a Class 100 clean room under laminar flow hoods. Sample filters were retrieved from storage at -80 ºC, removed from cryovials using plastic acid-washed forceps, and transferred into trace metal clean 15 mL PFA vials with 4 mL of 5% HNO_3 (Optima) containing a 1 ppb Indium (In) internal standard. Filters were digested for ~3.5h at 140 ºC using a HotBlock® heating block (Environmental Express, USA). Filters were then removed and discarded, leaving behind the liquid extract. After evaporating the remaining solution to just dryness, the residue was resuspended in 2 mL of 5% HNO_3 (Optima) by light vortexing. Process blank filters were digested and processed as sample filters were. Digests were analyzed in duplicate by ICP-MS using a Thermo ICAP-Q plasma mass spectrometer calibrated to a multi-element standard curve (Spex Certiprep) over a range of 1 – 20 ppb. Natural Cd and Zn isotope abundances of the standards were assumed to calculate concentrations of ^{110}Cd, ^{111}Cd, ^{114}Cd, ^{67}Zn, ^{66}Zn, and ^{68}Zn. Digests were analyzed in KED mode after an 85s sample uptake window and element mass windows were scanned 3 times during measurements. The 1 ppb In internal standard was used to correct for variation in sample delivery and plasma suppression between samples. Process blanks were subtracted from measured sample concentrations. Phosphorus

https://doi.org/10.5194/egusphere-2024-2085
Preprint. Discussion started: 2 August 2024

concentrations were simultaneously measured by ICP-MS and were calibrated to a standard curve ranging from 100 – 3,200 ppb using a 1 ppm certified P stock (Alfa Aesar Specpure). Equation #2 was used for the calculations described above:

$$M_{\text{particulate}} = \left[\frac{M_{sample}}{In_{sample}} - \frac{M_{blank}}{In_{blank}}\right] * \frac{In_{digestion}}{M_{slope}} * \frac{V_{digested}}{V_{filtered}} \quad (2)$$

where V_{filtered} is the total spiked sample volume estimated to have passed through the filter (275 mL), V_{digested} is the final volume the sample was resuspended in (2.0 mL), M_{sample} is the metal of interest measured in the sample in units of counts per second (cps), M_{blank} is the metal of interest measured in the process blanks (cps), M_{slope} is the slope of the metal of interest obtained by the standard curve (cps ppb^{-1}), In_{sample} is the In measured in the sample (cps), In_{blank} is the In measured in the process blanks (cps), $In_{\text{digestion}}$ is the cps of In measured in the 5% HNO_3+1 ppb In digestion solution, and the calculated concentration of the metal of interest ($M_{\text{particulate}}$) is in ppb (μg L^{-1}). This equation is the same as that used by Noble et. al. 2013 for the determination of particulate metal concentrations using ICP-MS (Noble et al. 2013).

The Zn spike and Cd spike were also analyzed by ICP-MS using a tenfold dilution of spike solution into 5% HNO_3 containing 1 ppb In to determine isotopic compositions and concentrations. When added to filled incubation bottles (275 mL total volume), the added concentrations were 288 pM ^{110}Cd, 4.51 pM ^{111}Cd, and 1.69 pM ^{114}Cd for Cd spiked bottles, and were 1.91 nM ^{67}Zn, 0.045 nM ^{66}Zn, and 0.047 nM ^{68}Zn for Zn spiked bottles (**Table S2**). For all stations and all depths, ^{67}Zn and ^{110}Cd spike concentrations exceeded natural dissolved ^{67}Zn and ^{110}Cd concentrations, estimated by multiplying the total dissolved Zn and Cd by the natural isotope abundance of ^{67}Zn and ^{110}Cd (0.0410 and 0.1249, respectively; see comparisons in **Fig. S2**).

2.6 Calculating zinc and cadmium uptake using ^{67}Zn and ^{110}Cd

https://doi.org/10.5194/egusphere-2024-2085
Preprint. Discussion started: 2 August 2024

Total Zn and Cd uptake was calculated using Eq. (3) and Eq. (4), respectively. $^{110}Cd_{Sample}$ and $^{67}Zn_{Sample}$ are the particulate ^{110}Cd and ^{67}Zn measured by ICP-MS analysis of the 3 µm sample filter (using the digestion protocol described in the prior section) normalized to the total culture volume (275 mL) and 24 hr of incubation. $^{110}Cd_{Sample}$ and $^{67}Zn_{Sample}$ already in the particulate fraction (that is, the pCd and pZn that existed in the water column upon collection of the raw seawater samples) were accounted for by subtracting these pre-existing particulate ^{110}Cd and ^{67}Zn values, $^{110}Cd_{PEP}$ and $^{67}Zn_{PEP}$. The pre-existing particulate value for ^{110}Cd was obtained from incubation bottles that had Zn added, but no Cd spike. Likewise, the pre-existing particulate value for ^{67}Zn was obtained from incubation bottles that had Cd added, but no Zn spike. The ^{67}Zn spike solution was confirmed to contain virtually no ^{110}Cd, ^{111}Cd, nor ^{114}Cd. The ^{110}Cd spike was likewise confirmed to contain virtually no ^{67}Zn, ^{64}Zn, nor ^{66}Zn. As a result, we assumed that the added ^{67}Zn spike did not affect the pre-existing Cd, nor did the ^{110}Cd spike affect the pre-existing Zn. It is assumed that the pre-existing particulate blank was in steady state, i.e. that it represented the Cd or Zn already in the particulate fraction and that any possible natural uptake that could occur during incubation for 24 h was negligible. The total dissolved pool of each metal isotope (denominator of each equation) is the sum of the dissolved ^{110}Cd or ^{67}Zn added as the spike ($^{110}Cd_{Spike}$, $^{67}Zn_{Spike}$) plus the natural, pre-existing dissolved ^{110}Cd or ^{67}Zn that was in the raw seawater ($^{110}Cd_{Natural}$, $^{67}Zn_{Natural}$) collected at each depth. To calculate $^{110}Cd_{Natural}$ and $^{67}Zn_{Natural}$, the total dissolved Cd or Zn measured by isotope dilution-ICP-MS (Cd_{Total}, Zn_{Total}) was multiplied by the natural abundance of ^{110}Cd and ^{67}Zn (12.49% and 4.10%, respectively). Dividing the particulate ^{110}Cd and ^{67}Zn by the total dissolved ^{110}Cd and ^{67}Zn yields the fraction of these metal isotopes that moved from the dissolved pool to the particulate pool per day (equation 3 and equation 4, respectively):

https://doi.org/10.5194/egusphere-2024-2085
Preprint. Discussion started: 2 August 2024

$$Cd_{total}\ Uptake\ Rate\ (pmol\ L^{-1}\ d^{-1}) = \frac{[^{110}Cd_{Sample}\ (pmol\ L^{-1}\ d^{-1}) - {}^{110}Cd_{PEP}\ (pmol\ L^{-1}\ d^{-1})]}{[^{110}Cd_{Spike}\ (pmol\ L^{-1}) + {}^{110}Cd_{Natural}\ (pmol\ L^{-1})]}\ x\ Cd_{total}\ (pmol\ L^{-1}) \quad (3)$$

$$Zn_{total}\ Uptake\ Rate\ (pmol\ L^{-1}\ d^{-1}) = \frac{[^{67}Zn_{Sample}\ (pmol\ L^{-1}\ d^{-1}) - {}^{67}Zn_{PEP}\ (pmol\ L^{-1}\ d^{-1})]}{[^{67}Zn_{Spike}\ (pmol\ L^{-1}) + {}^{67}Zn_{Natural}\ (pmol\ L^{-1})]}\ x\ Zn_{total}\ (pmol\ L^{-1}) \quad (4)$$

2.7 Nutrient analyses

Seawater samples taken for macronutrient analysis were filtered through 0.2 μm Supor (Pall) membrane filters and frozen at sea in acid-washed 60-mL high-density polyethylene (HDPE) bottles until analysis. Nutrient analyses were conducted by nutrient autoanalyzer by Joe Jennings at Oregon State University using previously described methods (Noble et al. 2012).

2.8 Statistics and plotting

Dissolved ecological stoichiometries were obtained from the slopes of two-way (type II) least squares linear regressions performed using the script lsqfitma.m rewritten from MATLAB to Python by Rebecca Chmiel (https://github.com/rebecca-chmiel/GP15). A correlation matrix of various parameters measured during NBP18-01 was created with SciPy v1.5.2 using the scipy.stats.pearsonr function, yielding Pearson correlation coefficients and p values that were visually represented using Seaborn v.0.11.1 and Matplotlib v3.3.2. Ocean sections were plotted using Ocean Data View v5.3.0 with gridded bathymetry file ETOPO1_2min. Outliers (see Data Availability) were excluded from ocean sectional plots. Mixed layer depth was calculated using the potential density function (pden) within the python-seawater module (v3.3.4). Figures were made using matplotlib (v3.3.2), Ocean Data View (v5.5.2), Excel (2019), and RStudio (v1.3.1093). ODV color palettes (https://doi.org/10.5281/zenodo.1243862) are inverse ‘roma’ for trace metal and macronutrient concentrations, ‘thermal’ for Zn and Cd uptake rates, and ‘algae’ for total fluorescence (Crameri 2023).

3 Results

3.1 Amundsen Sea

https://doi.org/10.5194/egusphere-2024-2085
Preprint. Discussion started: 2 August 2024

Zn and Cd uptake rate experiments were conducted at 18 stations. We define 3 groups of stations based on location: the Amundsen Sea, Ross Sea, and Terra Nova Bay (TNB) groups (**Fig. 1**). Uptake rates were assessed at 3 stations (4, 11 and 15) within the Amundsen Sea group, 6 stations (20, 29, 32, 35, 62, and 67) within the Ross Sea group, and 9 stations (22, 27, 41, 46, 52, 57, 72, 76 and 79) within the TNB group spanning ~10 – 250 m depth for a total of 18 stations and 125 samples. An overall schematic detailing these experiment workflows is shown in **Fig. 2.** The experimental design was validated by comparison of surface particulate ^{67}Zn:^{68}Zn and ^{110}Cd:^{114}Cd ratios measured in spiked samples with those measured in control (unspiked) samples. Samples spiked with ^{67}Zn had particulate ^{67}Zn:^{68}Zn ratios larger than natural abundance ratios at all stations (as was also true for ^{110}Cd spiked samples and Cd natural abundances; **Fig. S1**), indicative of uptake of the spike into the particulate phase.

The Amundsen Sea stations represented a linear cruise track, and we report total dissolved metal concentrations ($dMetal_T$) and uptake rates (ρMetal) over time in order of station sampling date (**Fig. 3a**).

https://doi.org/10.5194/egusphere-2024-2085
Preprint. Discussion started: 2 August 2024

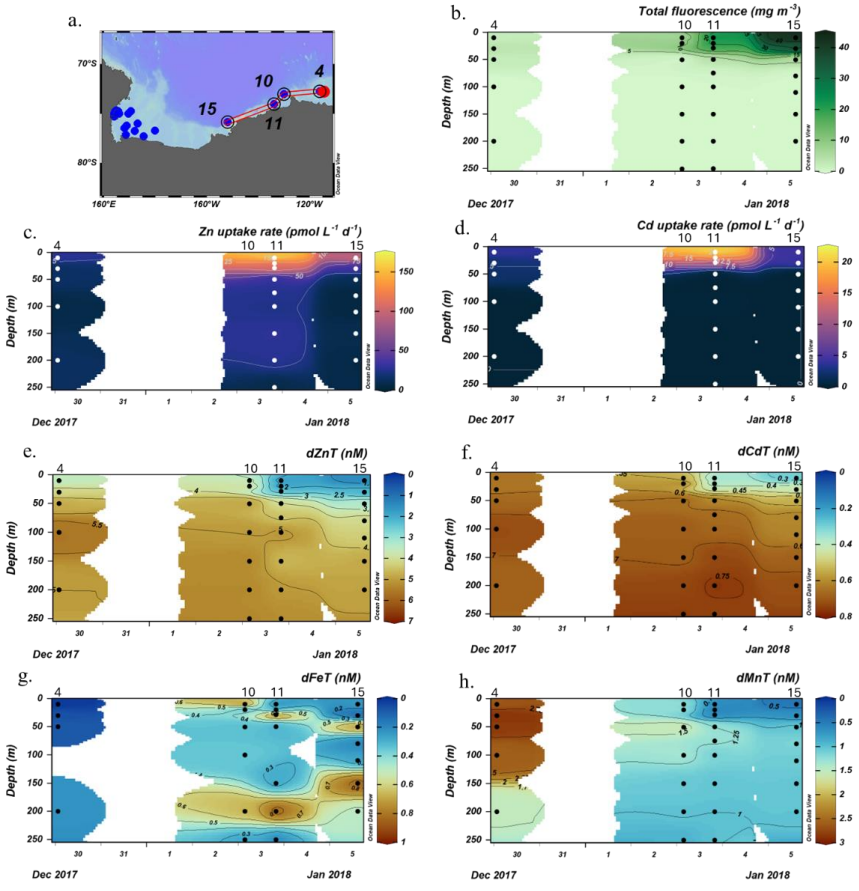

Figure 3. Total fluorescence and trace metal concentrations measured at Amundsen Sea stations shown over time. (a) Map showing station locations, (b) total chlorophyll (Chl) fluorescence, (c) total Zn uptake rates, (d) total Cd uptake rates, (e) total dissolved Zn, (f) total dissolved Cd, (g) total dissolved Fe, and (h) total dissolved Mn measured in the upper 250 m represented in color scale. Uptake experiments were not performed at station 10. Metal concentrations measured to 500 m depth are shown in Figure S3. dZnT, total dissolved Zn; dCdT, total dissolved Cd; dFeT, total dissolved Fe; dMnT, total dissolved Mn.

Among these stations, total Chl fluorescence was lowest at station 4 and increased moving westward along the transect to a Chl maximum of 41.8 mg m^{-3} at station 15, 10 m (**Fig. 3b**). Maximum surface concentrations of dZn, dCd and dMn were highest at station 4 (3.5 nM, 639 pM, and 2.6 nM at 10 m, respectively; **Fig. 3e, f, h**), likely reflecting the relatively smaller

https://doi.org/10.5194/egusphere-2024-2085
Preprint. Discussion started: 2 August 2024

amount of total biomass (as indicated by total Chl fluorescence; **Fig. 3b**) at this station. Concentrations of dZn, dCd and dMn decreased moving westward along the transect (**Fig. 3e, f, h**) as total Chl fluorescence increased (**Fig. 3b**). Total Zn uptake rates (ρZn) and total Cd uptake rates (ρCd) were highest at station 11 (158 and 21 pmol L^{-1} d^{-1}, respectively, at 10 m; **Fig. 3c,d; Fig. 4b**). Among the three Amundsen Sea stations, the largest movement of both Zn and Cd into the particulate phase therefore occurred at station 11, concurrent with the relatively higher dFe_T surface values observed at station 11 (0.2 nM dFe compared to 0.01 nM at station 4, 10 m; **Fig. 3g, Fig. S3c**). The dFe concentrations exceeding 1 nM near the seafloor are consistent with a sedimentary or subglacial source (**Fig. S3c**). Overall, ρZn and ρCd profiles exhibited trends in which values were highest within the upper 50 m at all three stations and decreased with depth, following the trend in Chl a or total Chl fluoresence (**Fig. 4**). Vertical sections of dZn and dCd through the water column mirrored these trends (**Fig. 4**), demonstrating the movement of these dissolved metal micronutrients into the particulate phase.

https://doi.org/10.5194/egusphere-2024-2085
Preprint. Discussion started: 2 August 2024

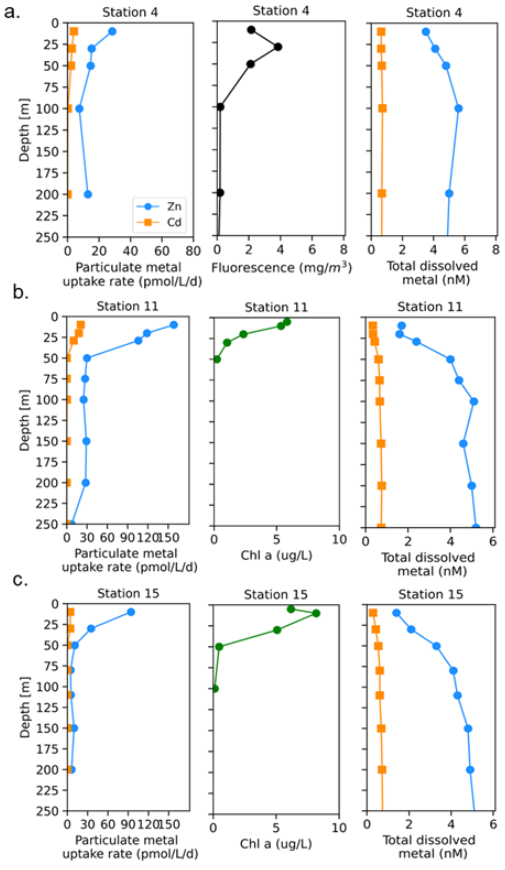

Figure 4. Depth profiles of total Zn and Cd uptake rates, total chlorophyll fluorescence (or chlorophyll *a*) and total dissolved metal measured in the upper 250 m at (a) station 4, (b) station 11, and (c) station 15 sampled along the Amundsen Sea shelf. Total chlorophyll (Chl) fluorescence is reported for stations where chlorophyll *a* (Chl a) data was not measured.

3.2 Ross Sea

We next investigated the dissolved Zn and Cd demand of the natural phytoplankton community at stations sampled over the Ross Sea shelf. Data collected from this group is presented over time, in order of sampling date (**Fig. 5**).

https://doi.org/10.5194/egusphere-2024-2085
Preprint. Discussion started: 2 August 2024

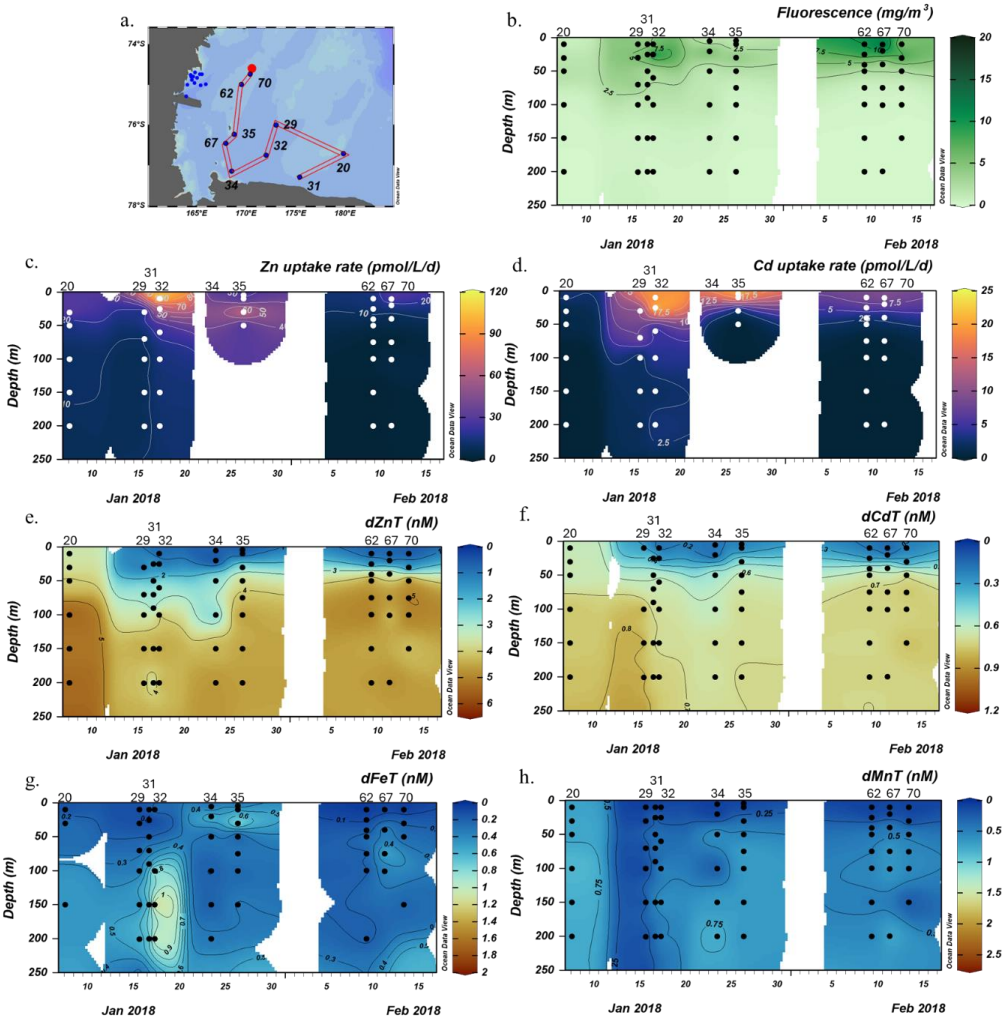

Figure 5. Total fluorescence and trace metal concentrations measured at Ross Sea stations shown over a latitudinal transect. (a) Map showing station locations, (b) total chlorophyll (Chl) fluorescence**,** (c) total Zn uptake rates, (d) total Cd uptake rates, (e) total dissolved Zn, (f) total dissolved Cd, (g) total dissolved Fe, and (h) total dissolved Mn measured in the upper 250 m represented in color scale. Uptake experiments were not performed at stations 31, 34, and 70. Metal concentrations measured to 800 m depth are shown in Figure S4. dZnT, total dissolved Zn; dCdT, total dissolved Cd; dFeT, total dissolved Fe; dMnT, total dissolved Mn.

We note that unlike the Amundsen Sea sector, the stations sampled in this group did not follow a linear cruise track, thus we cannot make inferences regarding latitudinal or longitudinal

https://doi.org/10.5194/egusphere-2024-2085
Preprint. Discussion started: 2 August 2024

changes. Surface Chl fluorescence was highest at stations 32 and 67 with maximum values of 15.8 and 14.6 mg m^{-3} at 25 m and 10 m, respectively (**Fig. 5b**). With the exception of station 20, dZn and dCd demonstrated high levels of surface depletion within the upper 25 m (**Fig. 5e,f**) with average concentrations of 0.63 ± 0.13 nM and 0.19 ± 0.09 nM respectively at ≤ 10 m. Compared to 100 m values (i.e., below the MLD), concentrations at 25 m were equivalent to 87%, 34%, 85%, 85%, 77%, and 88% decreases in dZn and 83%, 19%, 84%, 67%, 64%, and 75% decreases in dCd at stations 32, 20, 67, 35, 29, and 62, respectively. Measured dMn concentrations were also highly depleted within the upper 250 m at all Ross Sea stations (average 10 m dMn = 0.18 ± 0.26 nM; **Fig. 5h**). While dFe was depleted within the upper 10 m at all stations (average dFe concentration at 10 m = 0.12 ± 0.12 nM), concentrations exceeding 1 nM were observed below 100 m at station 32 (**Fig. 5g**) and extended down to 650 m (**Fig. S4c**), implying a sedimentary source. The largest Zn uptake rate measured among all stations in this group (115 pmol L^{-1} d^{-1}) was observed at station 32, 10 m (**Fig. 6c**). As observed in the Amundsen Sea, ρZn, ρCd and total Chl a or Chl fluorescence profiles exhibited surface maxima and became depleted with depth and were again mirrored by nutrient-like dZn and dCd depth profiles (**Fig. 6**), indicative of uptake of these metals into the particulate phase in surface waters.

https://doi.org/10.5194/egusphere-2024-2085
Preprint. Discussion started: 2 August 2024

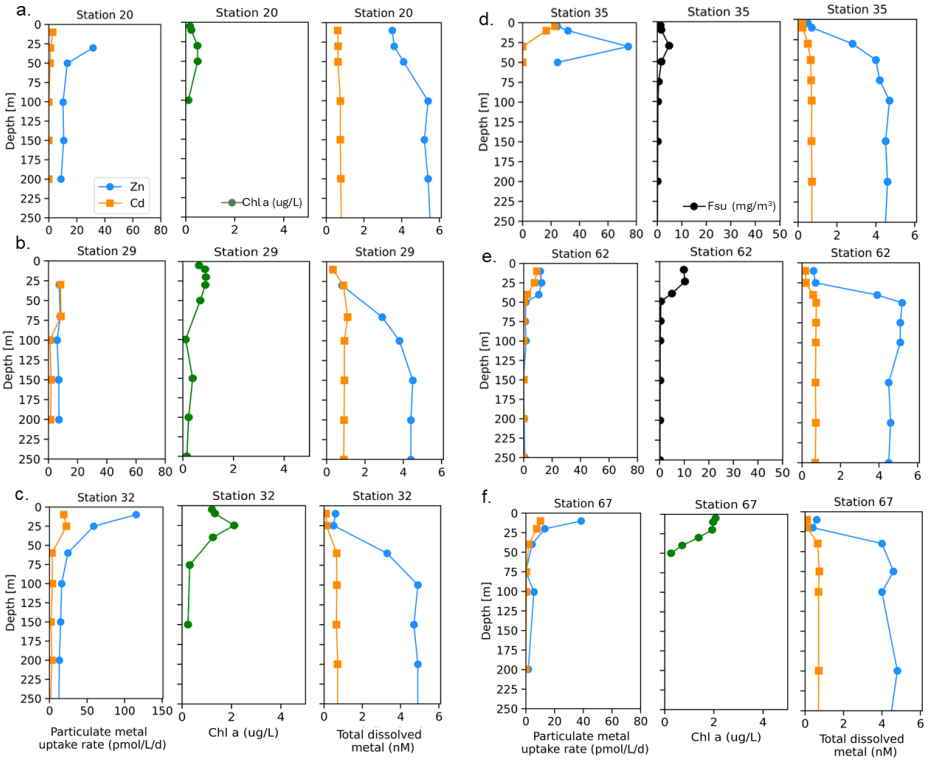

Figure 6. Depth profiles of total Zn and Cd uptake rates, total chlorophyll fluorescence (or, where available chlorophyll a), and total dissolved metal ($dMetal_T$) measured in the upper 250 m at (a) station 20, (b) station 29, (c) station 32, (d) station 35, (e) station 62, and (f) station 67 sampled along the Ross Sea shelf. Total chlorophyll (Chl) fluorescence is reported for stations where chlorophyll a (Chl a) data was not measured.

3.3 Terra Nova Bay

Zinc and Cd uptake rate data collected from stations sampled in Terra Nova Bay (TNB) were visualized over time due to repeated sampling within a small geographic region and similar timeframe (**Fig. 7a**). This allowed for an analysis of how dissolved metal concentrations and metal uptake rates changed throughout January-February 2018 within the same spatial area. Station data is presented in order of sampling date, from the earliest (station 22, sampled in early January) to the latest (station 79, sampled in late February).

https://doi.org/10.5194/egusphere-2024-2085
Preprint. Discussion started: 2 August 2024

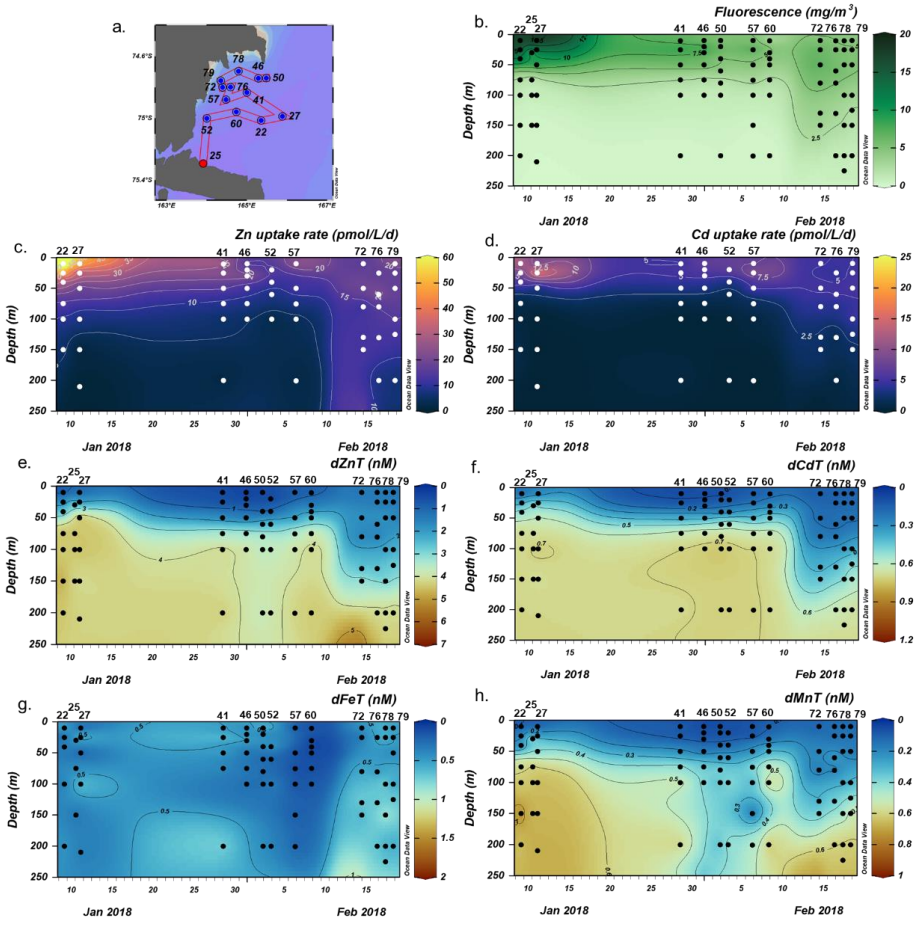

Figure 7. Total fluorescence and trace metal concentrations measured at Terra Nova Bay (TNB) stations shown over time. (a) Map showing station locations, (b) total chlorophyll (Chl) fluorescence, (c) total Zn uptake rates, (d) total Cd uptake rates, (e) total dissolved Zn, (f) total dissolved Cd, (g) total dissolved Fe, and (h) total dissolved Mn measured in the upper 250 m represented in color scale. Uptake experiments were not performed at stations 70 and 34. Metal concentrations measured to 600 m depth are shown in Figure S5. dZnT, total dissolved Zn; dCdT, total dissolved Cd; dFeT, total dissolved Fe; dMnT, total dissolved Mn.

Surface Chl fluorescence was highest in early January (~18 mg m^{-3}) and waned into February (**Fig. 7b**), similar to observed trends in Zn and Cd uptake rates (**Fig. 7 c,d**). Of all TNB stations, stations 22 and 27, sampled in January, had the highest maximum Zn uptake rates of 89.9 pmol L^{-1} d^{-1} and 46.0 pmol L^{-1} d^{-1}, respectively, at 10 m (**Fig. 8a,b**). Cd uptake rates were

https://doi.org/10.5194/egusphere-2024-2085
Preprint. Discussion started: 2 August 2024

also highest at these stations with values of 13.4 pmol L^{-1} d^{-1} and 20.1 pmol L^{-1} d^{-1} (**Fig. 8a,b**). At the final station (station 79, sampled in late February) maximum uptake rates of both metals had sharply decreased to 24.7 pmol Zn L^{-1} d^{-1} and 5.0 pmol Cd L^{-1} d^{-1} (**Fig. 8i**). Overall, maximum uptake rates of both metals decreased over time within TNB (**Fig. 7c,d**), consistent with the decrease in total Chl fluorescence (**Fig. 7b**) likely due to the aging and decline of the phytoplankton bloom.

Surface depletion of dZn, dCd, and dMn was observed at all stations with average dissolved concentrations of 0.82 ± 0.47 nM Zn, 0.13 ± 0.06 nM Cd, and 0.08 ± 0.04 nM Mn at 10 m depth (**Fig. 7e,f,h**). Notably, increased surface concentrations of dZn, dCd, and dMn were apparent at the late stations 72, 76, 78 and 79, with dZn ~2 nM, dCd ~300 pM, and dMn ~0.2 nM (**Fig. 7e,f,h; Fig. S5**). Dissolved macronutrient (phosphate, nitrate and nitrite, and silicate) concentrations also followed this trend, with increased surface concentrations at the late stations (**Fig. S6**). As with the Amundsen and Ross Sea station groups, Zn and Cd uptake rates within TNB tended to be highest at the surface ≤ 50 m as also observed in total Chl fluorescence trends and mirrored the decrease in total dissolved Zn and Cd (**Fig. 8**). Unlike the Amundsen and Ross Sea stations, where Cd uptake consistently became negligible (~0 pM L^{-1} d^{-1}) by 100 m (**Fig. 4**; **Fig. 6**), measurable Cd uptake persisted in TNB to 150 m at stations 72 and 79 (**Fig. 8g,i**). Measurable Zn uptake rates were also captured at deeper depths at these late TNB stations (**Fig. 8g,h,i**).

https://doi.org/10.5194/egusphere-2024-2085
Preprint. Discussion started: 2 August 2024

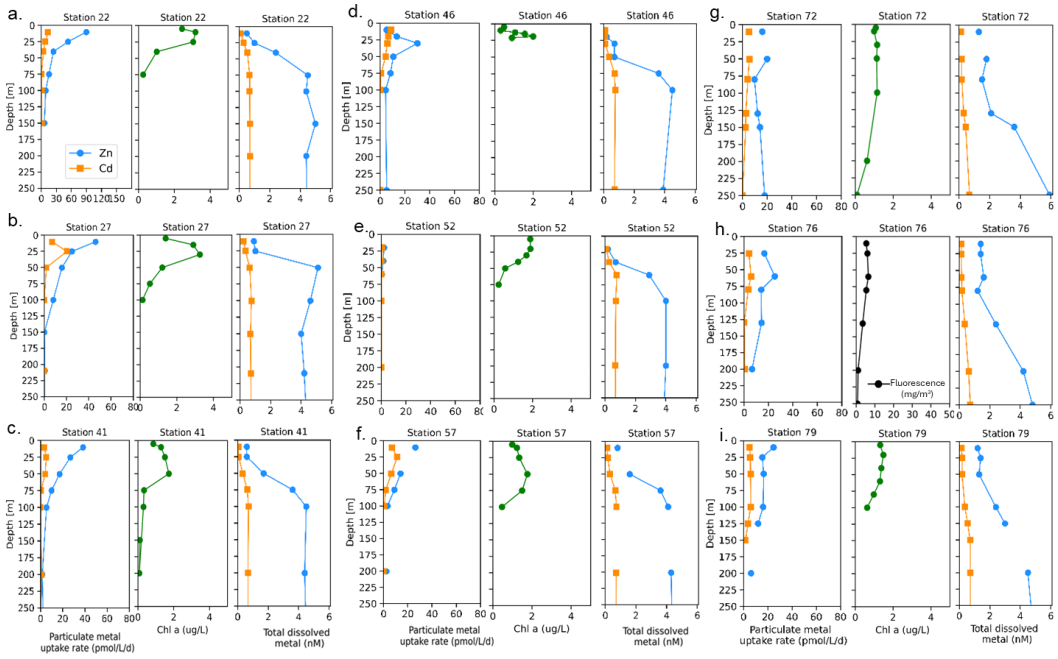

Figure 8. Depth profiles of total Zn and Cd uptake rates, total chlorophyll fluorescence (or, where available, chlorophyll a), and total dissolved metal (dMetalT) measured in the upper 250 m at (a) station 22, (b) station 27, (c) station 41, (d) station 45, (e) station 52, (f) station 57, (g) station 72, (h) station 76, and (i) station 79 within Terra Nova Bay. Total chlorophyll (Chl) fluorescence is reported for stations where chlorophyll a (Chl a) data was not measured.

The increased surface concentrations of dZn and dCd and macronutrients, as well as the persistence of measurable uptake rates at deeper depths, at these late TNB stations may be attributed to the deepening of the mixed layer (**Fig. S7**). Vertical mixing was evidenced by more uniform potential densities, temperatures, dissolved oxygen (O_2) concentrations, salinity, and beam transmission measurements at the late TNB stations within the upper 200 m (**Fig. S7**). Higher (>0.5 nM) dFe concentrations were also observed below 100 m at these late stations (**Fig. 7g**) and increased with depth (>2 nM), as did dZn and dMn concentrations, possibly due to sedimentary inputs (Giordano et al. 1999) (**Fig. S5**). At these late stations (Station 76, 78, 79) mixing replenished surface concentrations of both macronutrients (**Fig. S6**) and dZn (**Fig. S5a**),

https://doi.org/10.5194/egusphere-2024-2085
Preprint. Discussion started: 2 August 2024

but dZn was replenished to a lower extent. For example, comparing 50 m "replenished" surface values of P, N+N, and Si to deepwater (200 m) values at Station 79, percent changes from deep to surface values were -0.35% for P, -0.30% for N+N, and -0.26% for Si (a % change of 0 would indicate complete replenishment; i.e, if values at 200 m and at 50 m were equal). In contrast, the percent change from deep (200m) to surface (50m) dZn at Stn79 was lower, -0.71%. Hence, dZn was apparently replenished to a lesser extent compared to macronutrients, which may reflect a sustained high demand for Zn generating a dearth of this micronutrient despite macronutrient replenishment.

4 Discussion

4.1 Overview of Zn and Cd uptake at 18 stations

Maximum Zn and Cd uptake rates observed at each station (all of which were observed at ≤ 10 m depth; **Fig. 9a,b**) with uptake rates normalized to Chl a (µg/L) as a proxy for biomass (**Fig. 9c,d).**

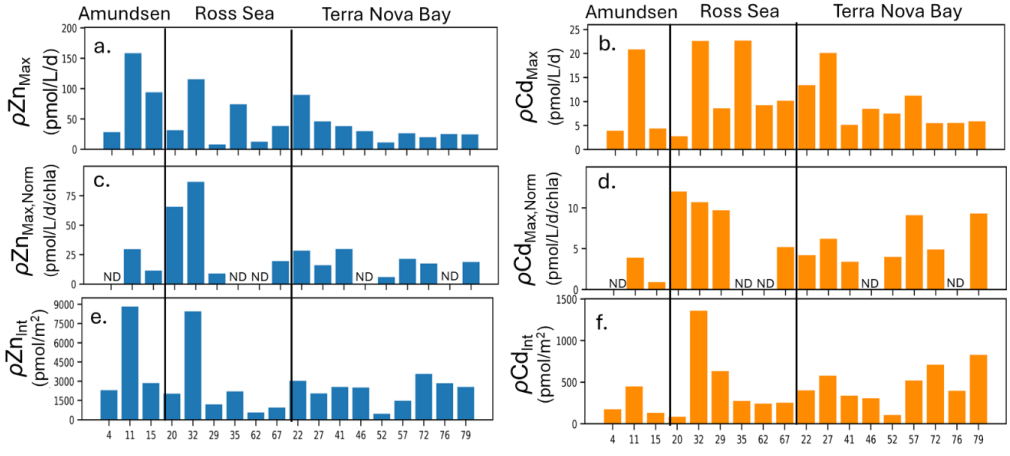

Figure 9. Unnormalized (a) maximum Zn uptake rates (ρZn_{Max}) and (b) maximum Cd uptake rates (ρCd_{Max}) at each station grouped by area (Amundsen Sea, Ross Sea, Terra Nova Bay). (c) ρZn_{Max} and (d) ρCd_{Max} normalized to chlorophyll a (µg L^{-1}) measured at each station. (e) Depth integrated (10 m-250 m) ρZn and ρCd values at each station. ND, no data (chlorophyll a not measured).

https://doi.org/10.5194/egusphere-2024-2085
Preprint. Discussion started: 2 August 2024

Overall, high (>25 pmol L^{-1} d^{-1} Chl a (ug/L) $^{-1}$) Chl a-normalized Zn uptake rates were measured at station 11 in the Amundsen Sea and at stations 20 and 32 in the Ross Sea (**Fig. 9c**). The highest Chl a-normalized Cd uptake rates among all 18 stations were also measured at stations 20 and 32 (**Fig. 9d**). Across TNB, Chl a-normalized maximum Zn and Cd uptake ranged from 6.0 – 28.3 pmol L^{-1} d^{-1} Chl a^{-1} for Zn, and 3.4 – 9.3 pmol L^{-1} d^{-1} Chl a^{-1} for Cd; **Fig. 9c,d**). Integrated (10 m-250 m) uptake rate values were highest for Zn at stations 11 and 32, and highest for Cd at station 32 (**Fig. 9e,f**). Increases in integrated Cd and Zn uptake at the late stations 72, 76 and 79 reflected the deeper depths to which uptake rates of these metals remained measurable, likely reflecting deepened mixed layers (**Fig. S7**) and/or sinking of the phytoplankton community, as seen in the fluorescence data to beyond 150m depth (**Fig. 7b**). The presence of Chl a (**Fig. 8g,i**) implies these deep phytoplankton communities may still be alive, if not actively photosynthesizing. We previously identified ZCRP-B, a membrane-associated protein involved in high-affinity Zn transport (Kellogg et al. 2022). These proteins have a single transmembrane domain, implying function as a membrane-tethered ligand to assist in the acquisition of Zn from seawater in cooperation with adjacent zinc transporters (ZIP transporters). Hence ZCRP-B could be a potential site of Zn binding and 'uptake', as our uptake rate measurements do not discern between extracellular and intracellular Zn, even if the phytoplankton are inactive due to a lack of photosynthetic energy at these depths.

4.2 Use of metal uptake rates to determine depletion timeframes

The measurement of total dissolved metal concentrations over large latitudinal or longitudinal areas allows for the characterization of metal inventories, though these are snapshots of inventories observed at specific times. The measurement of metal uptake rates allows us to gain new insight into how these inventories came to be and the timeframes over which they are

https://doi.org/10.5194/egusphere-2024-2085
Preprint. Discussion started: 2 August 2024

consumed and replenished. Due to the resetting of surface dissolved metal concentrations to those of deepwater values during austral winter with deep winter mixing, the Ross Sea of the Southern Ocean is particularly applicable to this type of timeframe study (Sedwick and DiTullio 1997; Sedwick et al. 2011).

Using the Zn uptake rates measured in this study, we can estimate the time required for the high levels of primary production observed in the Southern Ocean to draw down surface dZn from high (deep water) winter concentrations to the surface concentrations observed during austral summer 2017. The Southern Ocean growing season typically spans October-March, with primary productivity peaking November-January and the area of open (ice-free) water over the Ross Sea shelf linearly increasing from November-mid January (Sedwick et al. 2011). Vertical profiles of nutrients and micronutrients in coastal Antarctic ecosystems such as the Ross Sea are reset and become uniform with depth during the winter months due to whole-water column mixing and an absence of photosynthetic activity during the dark winter under the sea ice (Noble et al. 2013). As a result, the drawdown of nutrients in the upper water column observed during the spring and summer seasons is the result of less than one year's biological influence. For this simple calculation, we ignore the upward flux of Zn (upwelling = 0) and assume a high export ratio of 0.8 due to bloom productivity being dominated by diatoms and *Phaeocystis antarctica*, both of which sink rapidly and thus contribute substantially to carbon export flux (Asper and Smith 1999; DiTullio et al. 2000). The depletion of dZn from a surface box was therefore estimated as:

$$\left(\frac{dZn}{dt}\right)_{surface\ box} = -\rho Zn + (Rf * \rho Zn) + upwelling$$

Where Rf is the remineralization factor equal to 1 - export ratio.

https://doi.org/10.5194/egusphere-2024-2085
Preprint. Discussion started: 2 August 2024

Taking station 11, for which the highest Zn uptake rate was observed, as an extreme case: with a maximum Zn uptake rate of 158 pmol L^{-1} d^{-1}, it would take only 25 days to deplete a surface winter concentration of 4.8 nM (that is, the average deepwater (< 200 m) dZn concentration for all stations measured in this study) down to the observed surface concentration of 1.7 nM at station 11, assuming a constant uptake rate and no additional inputs of dissolved Zn (**Fig. 10**).

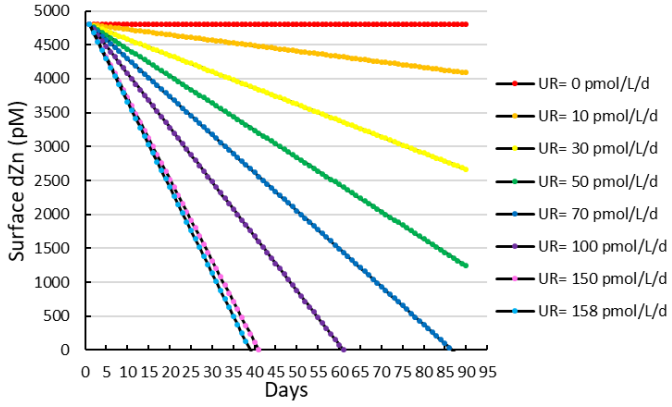

Figure 10. A simple model estimating the time (in days) required to deplete the estimated average winter surface concentration of dZn (4.8 nM) over a range of various Zn uptake rates (UR). 158 pmol/L/d was the maximum Zn uptake rate observed in this study (station 11, 10 m).

Given that dZn surface depletion to sub-nanomolar levels was observed throughout much of the CICLOPS expedition, prolonged high levels of Zn uptake and export that overwhelm replenishment by vertical mixing and/or remineralization are likely key to giving rise to the observed extent of seasonal surface dZn depletion. These calculations were conducted as a proof-of-concept to determine if uptake rates were sufficient to draw down the otherwise abundant dZn inventory on seasonal timescales. Future studies could conduct mesoscale modeling of the region, replacing upwelling including eddy diffusion and advection. Notably, any dZn upwelling

https://doi.org/10.5194/egusphere-2024-2085
Preprint. Discussion started: 2 August 2024

flux into the euphotic zone would require even higher Zn uptake rates to create the seasonal surface Zn depletion we observed on this expedition.

4.3 Influences on Zn and Cd uptake

We next consider the factors driving the magnitude of ρZn and ρCd. As noted above, ρZn and ρCd were positively correlated with total Chl fluorescence or Chl a at every station (**Fig. 4; Fig. 6; Fig. 8**), demonstrating the influence of total autotrophic biomass on uptake rates. A Pearson correlation analysis comparing the abundance of individual algal pigments to ρZn and ρCd throughout the water column for all stations revealed significant, positive correlations (Pearson correlation coefficient > 0.50, $p \leq 1.2e\text{-}4$) between ρZn and Chl *a*, Chl *b*, and Chl c1, c2 and c3. Pearson correlation coefficients are normally symbolized as rho (ρ), but to avoid confusion with our uptake symbol (ρ), and with p-values (p), they are herein referred to as 'cc' values. The correlation between ρZn and Chl *b* was strongest (cc= 0.77, p = 3.8e-10) of any pigment (**Fig. 11e**).

https://doi.org/10.5194/egusphere-2024-2085
Preprint. Discussion started: 2 August 2024

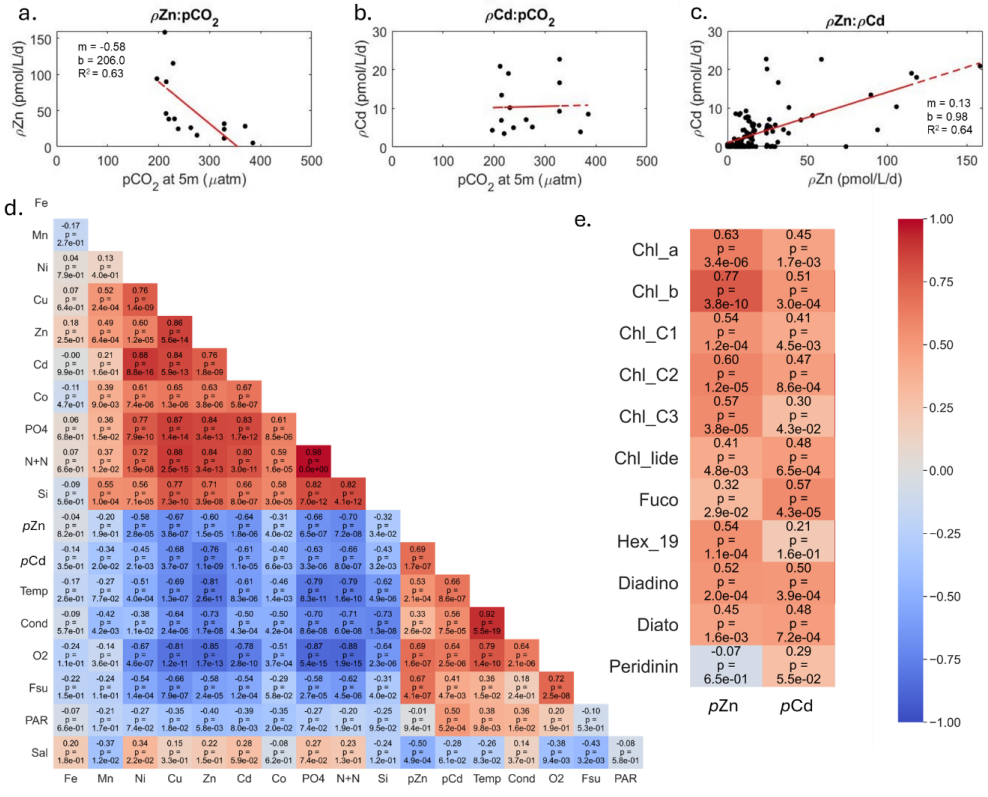

Figure 11. Relationships comparing seawater CO_2 partial pressure (pCO_2) at 5 m depth to (a) Zn uptake rates (ρZn; n=15, R^2 = 0.63) and (b) Cd uptake rates (ρCd; n=15) measured at surface (≤10 m) depths. (c) Relationship between ρZn and ρCd for all depths (n=121, R^2 = 0.64). (d) Visual representation of the correlation matrix comparing all water column parameters measured with depth with warm and cool colors indicative of positive and inverse correlations, respectively. Pearson correlation coefficients and p values are shown. (e) Representation of the correlation matrix comparing ρZn and ρCd to various phytoplankton pigments. Fe, Mn, Ni, Cu, Zn, Cd, and Co labels correspond to total dissolved metal concentrations. PO4, N+N, and Si correspond to total dissolved concentrations of phosphate, the sum of nitrate+nitrite, and silicate. Temp, temperature; cond, conductivity; O_2, dissolved oxygen; Fsu, total fluorescence; PAR, photosynthetically active radiation; Sal, salinity. Chl_a, chlorophyll *a*; Chl_b, chlorophyll *b*; Chl_c1, chlorophyll c1; Chl_c2, chlorophyll c2; Chl_c3, chlorophyll c3; chl_lide, chlorophyllide; Fuco, fucoxanthin; Hex_19, 19'-hexanoyloxyfucoxanthin; Diadino, diadinoxanthin; Diato, diatoxanthin.

In bottle incubation experiments conducted at station 27, the addition of Zn alone resulted in the positive growth response of Chl *b*-containing algae (small green algae such as

https://doi.org/10.5194/egusphere-2024-2085
Preprint. Discussion started: 2 August 2024

prasinophytes; (Kell et al. 2023), corroborating this finding. ρCd also positively correlated with these Chl pigments but with slightly lower correlation Pearson correlation coefficients (cc = 0.3-0.51; $p \leq .043$). Fucoxanthin (fuco) concentrations were more highly correlated with ρCd (cc = 0.57, p = 4.3e-5) than with ρZn (cc = 0.32, p =2.9e-2), while the opposite was observed for 19'-Hex (19'-hexanoyloxyfucoxanthin; cc = 0.54, p = 1.1e-4 for Zn; not significant for Cd) (**Fig. 11e**). Fuco and 19'-Hex are used as taxonomic indicators of diatoms and *Phaeocystis*, respectively, in the Ross Sea (DiTullio and Smith 1995; DiTullio et al. 2003, 2007; Wright et al. 2010). The higher correlation coefficient between ρZn and *Phaeocystis* abundance (as indicated by 19'-Hex) implies that Zn uptake was driven largely by *Phaeocystis*. This finding is consistent with the detection of *Phaeocystis* ZCRP-A, a protein characterized as an algal Zn^{2+} metallochaperone (Kellogg et al. 2022), in metaproteomic data collected from both the incubation experiment and throughout the water column at station 27 (Kell et al. 2023). The positive correlation between ρCd and the abundance of diatoms (as indicated by fuco) is consistent with the diatomic utilization of Cd as a nutrient within CDCA metalloenzymes, as *cdca* genes have, to date, been found exclusively in diatom species (Park et al., 2007, 2008). While it is likely that both *Phaeocystis* and diatoms contributed to the Cd and Zn uptake rates measured here, it is currently unknown if *Phaeocystis* can utilize Cd as a nutrient. Overall, any potential growth benefit conferred by our Cd spike additions may only have been applicable to diatoms that 1) possessed the *cdca* gene and 2) faced selection pressure to utilize Cd as a cofactor in CDCA due to low seawater pCO_2 (as documented on this expedition) creating enhanced demand for dZn. The presence of Cd-utilizing diatoms in the water column at station 27 was demonstrated by the detection of CDCA transcripts with closest taxonomic matches to the diatom genera *Chaetoceros* and *Corethron* (Kell et al. 2023). Station 27 also exhibited high

https://doi.org/10.5194/egusphere-2024-2085
Preprint. Discussion started: 2 August 2024

surface Chl fluorescence (19.3 mg m^{-3} at 10 m), low pCO_2 (221 µatm at 5 m), and high maximum Zn and Cd uptake rates (46 and 20 pmol L^{-1} d^{-1}, respectively), demonstrating a high algal demand for Zn that likely created pressure for Cd uptake.

We next consider the effect of the depleted seawater pCO_2 levels induced by the high biomass conditions observed on this expedition. Previously, a strong correlation between dissolved $\delta^{114}Cd$ and dissolved CO_2 was documented in the Atlantic Sector of the Southern Ocean (de Baar et al. 2017), suggesting significant Cd isotope fractionation due to biological uptake into the particulate phase. A relationship between total surface Cd uptake rates at 10 m and surface pCO_2 (underway, measured at 5 m) was not observed in the present study (**Fig. 11b**). The present study includes measurements of total Cd uptake (that is, the sum of all Cd isotopes) using an added Cd isotope tracer, and hence did not explore natural isotope fractionation effects. However, we did observe a significant negative linear relationship between total Zn uptake rates and seawater pCO_2 (m = -0.58; R^2 = 0.63; **Fig. 11a**) consistent with an increased demand for Zn^{2+} to power the carbon concentrating mechanism of photosynthetic algae under lower CO_2 availability. ρZn and ρCd furthermore shared a significant positive linear relationship with each other (m = 0.13; R^2 = 0.64; **Fig. 11c**) (as was also reflected in the Pearson correlation test; PCC = 0.69, p = 1.7e-7, **Fig. 11d**) implying that as demand for Zn increased, demand for Cd also increased, consistent with laboratory studies showing their co-transport in marine algae (Sunda and Huntsman 2000). We also note that ρCd:ρZn uptake ratios were higher (> 0.4) at the surface where total dissolved dCd:dZn ratios were comparatively higher (> 0.3) (**Fig. 12a,b**). The strong positive linear relationship shared between these ratios (R^2 = 0.82; **Fig. 12c**) further suggests that dZn levels were depleted enough to induce increased Cd uptake rates, and is consistent with their known biochemical substitution within marine algae.

https://doi.org/10.5194/egusphere-2024-2085
Preprint. Discussion started: 2 August 2024

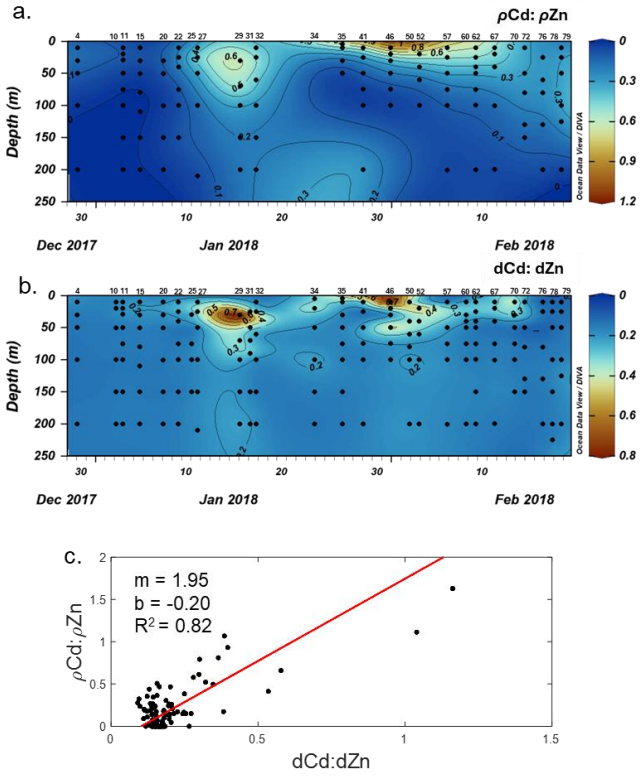

Figure 12. (a) Cd:Zn uptake ratios (ρCd:ρZn) and (b) total dissolved Cd:Zn ratios (dCd:dZn) for all stations during the CICLOPS expedition measured in the upper 250 m represented in color scale and over time of sampling. (c) Two-way linear regression showing the positive relationship between dCd:dZn and ρCd:ρZn inclusive of all stations and depth (n=111, R^2 = 0.82).

Algal Cd uptake rates are known to be inversely related to both Mn^{2+} and Zn^{2+} concentrations in culture (Lee et al. 1995; Sunda and Huntsman 1996), which is thought to reflect the uptake of Cd by two separate inducible transport systems. Cadmium is taken up competitively by the high-affinity Zn uptake system under low Zn^{2+} conditions, as demonstrated above, while Cd, Zn, and Mn share the same low-affinity Mn uptake system under high Zn^{2+} conditions (Lee et al. 1995; Sunda and Huntsman 1998a; b, 2000; Xu et al. 2007). With the exception of the Amundsen Sea stations, dMn was consistently observed at concentrations of only 0.1-0.5 nM within the upper 50 m (**Fig. 3h; Fig. 5h; Fig. 7h).** Low surface dMn

https://doi.org/10.5194/egusphere-2024-2085
Preprint. Discussion started: 2 August 2024

concentrations within the Southern Ocean have been documented previously and were attributed to a combination of biological uptake at the surface causing depletion and low resupply due to few external sources (Latour et al. 2021). While ρCd was negatively correlated with dMn (PCC = -0.34, p = 0.02) considering all stations and all depths, ρCd was more strongly negatively correlated with dZn (PCC = -0.76, p = 1.1e-9), which was the strongest negative correlation comparing all measured parameters to ρCd (**Fig. 11d**). This finding is consistent with decreased dCd uptake where dZn availability is sufficient. Overall, these results are consistent with biology (total biomass) and pCO_2 acting as primary influences on ρZn, with increases in ρZn leading to increases in ρCd through the upregulation of a shared transport system.

4.4 dZn and dCd relationships with macronutrients

The growth of phytoplankton and bacteria in the shallow euphotic zone results in the removal of bioactive trace metals and macronutrients from the dissolved phase into the particulate phase, resulting in dissolved metal:macronutrient relationships that reflect their collective stoichiometry (Horner et al. 2021). Positive linear slopes result generally indicate the co-cycling of the metal and the macronutrient via uptake and remineralization, though slope values can vary widely by basin as they are a function of the metal:macronutrient uptake and remineralization stoichiometry of the native community and overall nutrient availability. Two-way linear regressions (see Methods) were used to investigate the relationships between dZn and dissolved silicate (dSi), dZn and dissolved phosphate (dP), and dCd and dP for the Amundsen Sea, Ross Sea, and TNB station groups (**Fig. 13**).

https://doi.org/10.5194/egusphere-2024-2085
Preprint. Discussion started: 2 August 2024

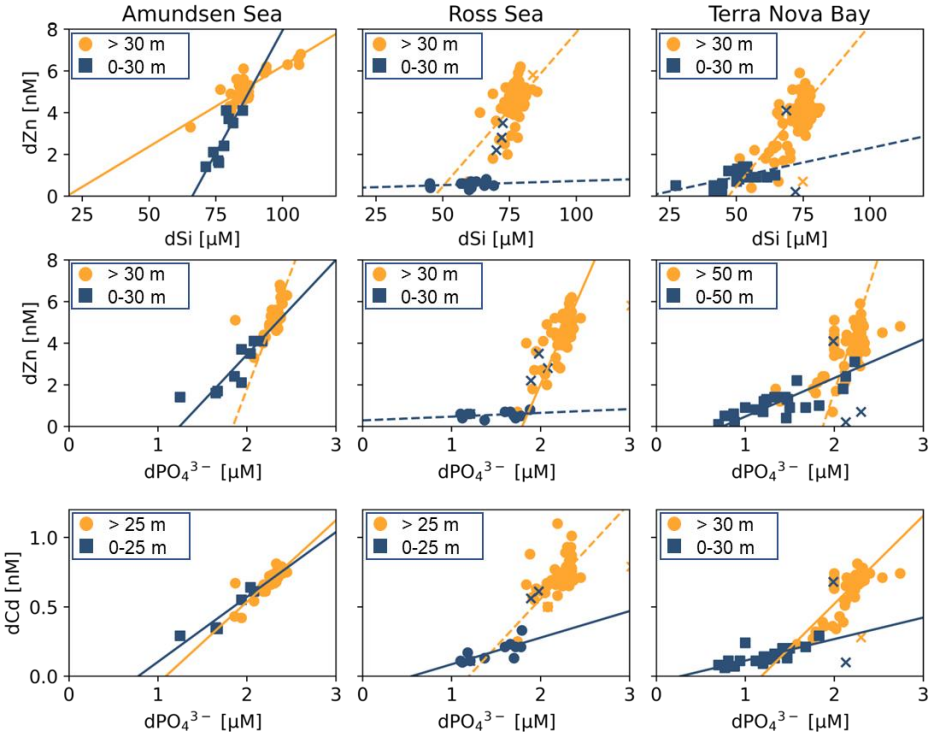

Figure 13. Relationships between (Top row) total dissolved Zn and silicate (dSi), (Middle row) total dissolved Zn and phosphate (dPO_4^{3-}), and (Bottom row) total dissolved Cd and dPO_4^{3-} for surface (blue squares) and deep ocean (orange circles) arranged by station group (Amundsen Sea, Ross Sea, and Terra Nova Bay). Depth thresholds were manually chosen to optimize the linear fit of the surface and deep ocean trends. Regressions with an $R^2 \geq 0.50$ are shown as a solid line, and those with an $R^2 < 0.50$ are shown as a dotted line. See **Table S4** for stoichiometric parameters and values. Regression outliers are marked with an 'x'. Data originally plotted in Chmiel et al. 2023 and reprised here for ease of comparison with dZn:Si data.

The dZn:dP and dCd:dP relationships from this expedition were originally presented in Chmiel et al. 2023 for comparison to dCo:dP, while they are included in the present study for ease of comparison with dZn:dSi relationships presented for the first time. For these analyses, the depth threshold that separates the surface and deep ocean was manually defined in order to optimize the linear fit of the surface versus deep trends— this threshold depth can be thought of

https://doi.org/10.5194/egusphere-2024-2085
Preprint. Discussion started: 2 August 2024

as an inflection point that represents the largest change in trace metal concentration with respect to dP or dSi concentration (Chmiel et al. 2023).

As noted above, the near-linear global dZn:dSi relationship (Bruland et al. 1978; Vance et al. 2017; Middag et al. 2019) has been posited to arise, in part, from faster drawdown of Zn and Si relative to dPO_4^{3-} into Southern Ocean diatoms that leaves surface waters Zn and Si depleted (Vance et al. 2017). We observed distinct differences in dissolved dZn:dSi ecological stoichiometries comparing Amundsen Sea, Ross Sea and Terra Nova Bay station groups (**Fig. 13; Table S4**). A positive linear dZn:dSi relationship with a steep ($m = 0.23 \pm 0.05$; **Table S4**) slope observed in the upper ocean of the Amundsen Sea contrasted starkly with the shallow slopes observed in the upper ocean of the Ross Sea and Terra Nova Bay. A bloom of non-silicifying *Phaeocystis antarctica* was present during our passage through the Amundsen Sea, consistent with abundant silicic acid yet rapid drawn down of Zn, which is known to be used by this organism (Saito and Goepfert 2008). In contrast, the shallow slopes in the Ross Sea and Terra Nova Bay resulted from the persistence of dSi concentrations ≥ 30 µM in the upper 30 m while dZn was reduced to sub-nanomolar concentrations (average $dZn = 0.87 \pm 0.42$ nM in TNB at 10 m depth, n= 11), highlighting the intense drawdown of dZn by biota in this region to meet a high metabolic dZn demand.

Similar trends were observed for dZn:dP and dCd:P, which exhibited shallow slopes within the upper ocean of the Ross Sea and Terra Nova Bay. Southern Ocean diatoms are known to have Zn:P uptake ratios that are up to an order of magnitude greater than the average for oceanic phytoplankton (Twining and Baines 2013; Vance et al. 2017; Sieber et al. 2020). The increased presence of diatoms (as indicated by higher fucoxanthin concentrations) at the late stations within Terra Nova Bay therefore likely exacerbated the surface decoupling of dZn and

https://doi.org/10.5194/egusphere-2024-2085
Preprint. Discussion started: 2 August 2024

dP due to their high dZn demand. The maximum uptake rates of 158, 115, and 89 pmol Zn L^{-1} d^{-1} measured in this study for the Amundsen Sea, Ross Sea, and Terra Nova Bay groups, respectively, contextualize the high Zn uptake rates hypothesized to contribute to the high dZn:dP uptake ratios observed in Southern Ocean diatoms. These rates are indicative of total potential biological uptake, likely influenced by a depleted labile Zn pool and residual of complexed Zn, that then results in low dZn:dP ratios in shallow waters.

Like dZn and dSi, dCd and dP concentrations are known to share strong correlations in both deep and surface seawater (Boyle et al. 1976; Boyle 1988; de Baar et al. 1994), with the vertical distribution of Cd controlled by phytoplankton uptake in surface waters and sinking of particulate organic matter and subsequent remineralization at depth. Observations of enhanced Cd uptake within the Fe-limited Southern Ocean (Cullen 2006) are consistent with observations of increased Cd uptake by marine algal species under Fe limitation in both the field (Cullen et al. 2003; Cullen and Sherrell 2005; Baars et al. 2014) and in culture (Sunda and Huntsman 2000; Lane et al. 2009), thought to be due to the increased use of Cd in biochemical processes or inadvertent uptake due to the upregulation of metal transporters (Sunda and Huntsman 2000; Cullen 2006). In these coastal regions, dCd:dP had the same regional and depth trends as dZn:dP, further demonstrating their close biogeochemical association.

5 Conclusions

We have quantified the movement of the trace metals Zn and Cd from the dissolved to the particulate phase within the phytoplankton >3 µm size fraction collected in the Amundsen Sea, Ross Sea, and Terra Nova Bay of the Southern Ocean during austral summer 2017-2018. Increases in particulate ^{110}Cd and ^{67}Zn concentrations in spiked samples, increases in particulate ^{67}Zn:^{68}Zn and ^{110}Cd:^{114}Cd sample ratios relative to controls, and surface depletion of total

https://doi.org/10.5194/egusphere-2024-2085
Preprint. Discussion started: 2 August 2024

dissolved Zn and Cd concentrations apparent at all 18 stations demonstrated metal uptake into the particulate phase mainly within the upper 50 m. Our study confirms the utility of the 24hr Cd stable isotope tracer uptake method employed previously (Cox et al. 2014) and expands its use to measurements of Zn uptake. Notably, maximum Cd uptake rates measured in the present study were 3.4, 3.7, and 3.3 times higher in the Amundsen Sea, Ross Sea, and Terra Nova Bay, respectively, compared to the maximum Cd uptake rate of 6.1 pmol L^{-1} d^{-1} measured previously within the Costa Rica Dome using identical methods (Cox et al. 2014), demonstrating the influence of high productivity and the native community on the flux of dCd into the particulate phase.

The highly productive phytoplankton bloom documented in the study area resulted in an intense algal Zn demand within the surface ocean, which we have quantified via uptake rate measurements. This intense Zn demand shifted the demand for other trace metal micronutrients as well, namely Cd and cobalt (Co) (Chmiel et al. 2023). Due to their similar charge and atomic radii, Zn^{2+}, Co^{2+} and Cd^{2+} cations often share the same transporter uptake systems. An organism's ability to utilize these metals as metabolic cofactors is influenced by their environment and the affinity of the uptake ligands for each metal cation (Irving and Williams 1953; Sunda and Huntsman 1992). When dZn availability is low, more dCd and dCo are able to bind transport ligands. Therefore, dZn concentrations and cycling can influence the cycling of dCd and dCo, particularly in low dZn environments as documented for dCd in the present study. The influence of dZn cycling on dCo distributions in this region was also documented for the same expedition, with evidence for high rates of biological Co uptake in the Ross Sea driven by dZn (and vitamin B_{12}) scarcity (Chmiel et al. 2023). The high Zn uptake rates measured in this study therefore not only demonstrate a mechanism for the depletion of abundant Zn in coastal

https://doi.org/10.5194/egusphere-2024-2085
Preprint. Discussion started: 2 August 2024

areas with the potential for Zn scarcity during highly productive bloom events, but also reveal dynamic changes in the cycling of Cd and Co as a consequence of high Zn demand.

Data availability

CICLOPS (NBP18-01) CTD hydrography data (including pressure, temperature, total dissolved oxygen, conductivity, fluorescence, and beam transmission; https://www.bco-dmo.org/dataset-deployment/783917) in addition to total dissolved metal, Zn and Cd uptake rate, macronutrient, and pigment datasets are available through the NSF Biological and Chemical Oceanography Data Management Office (BCO-DMO) repository (https://www.bco-dmo.org/deployment/778919). Underway pCO_2 data collected during cruise NBP1801 is available through R2R, https://doi.org/10.7284/139318.

Author contributions

Conceptualization and analysis of the study was carried out by RMK and MAS. This work was supervised by MAS and GRD. Funding was acquired by MAS and GRD. All co-authors contributed to data collection. RMK and MAS wrote the manuscript with review and editing contributions from all co-authors.

Competing interests

The authors declare that they have no conflict of interest.

Acknowledgements

We thank the captain, crew, marine technicians, and science party of RVIB Nathaniel B. Palmer for their support and contributions to the success of the NBP18-01 cruise, Joe Jennings (OSU) for conducting macronutrient analyses, Lauren Lees for assistance with sampling, and Natalie Cohen for assistance in operation of the seaFAST and application of the isotope dilution technique.

https://doi.org/10.5194/egusphere-2024-2085
Preprint. Discussion started: 2 August 2024

Funding

National Science Foundation grant 2123055 (MAS)

National Science Foundation grant 2125063 (MAS)

National Science Foundation grant 1643684 (MAS)

National Science Foundation grant 1924554 (MAS)

National Science Foundation grant NSF-PLR 1643845 (RBD)

Simons Foundation (MAS)

National Science Foundation grant NSF-OPP 1644073 (GRD)

TJH acknowledges support from the Woods Hole Oceanographic Institution's *Ocean and Climate Innovation Accelerator* program.

References

Arrigo, K. R., G. L. van Dijken, and S. Bushinsky. 2008. Primary production in the Southern Ocean, 1997–2006. Journal of Geophysical Research **113**: C08004. doi:10.1029/2007JC004551

Arrigo, K. R., K. E. Lowry, and G. L. van Dijken. 2012. Annual changes in sea ice and phytoplankton in polynyas of the Amundsen Sea, Antarctica. Deep Sea Research Part II: Topical Studies in Oceanography **71–76**: 5–15. doi:10.1016/j.dsr2.2012.03.006

de Baar, H. J. W., S. M. A. C. van Heuven, W. Abouchami, Z. Xue, S. J. G. Galer, M. Rehkämper, R. Middag, and J. van Ooijen. 2017. Interactions of dissolved CO2 with cadmium isotopes in the Southern Ocean. Marine Chemistry **195**: 105–121. doi:10.1016/J.MARCHEM.2017.06.010

de Baar, H. J. W., P. M. Saager, R. F. Nolting, and J. van der Meer. 1994. Cadmium versus phosphate in the world ocean. Marine Chemistry. doi:10.1016/0304-4203(94)90082-5

https://doi.org/10.5194/egusphere-2024-2085
Preprint. Discussion started: 2 August 2024

839 Baars, O., W. Abouchami, S. J. G. Galer, M. Boye, and P. L. Croot. 2014. Dissolved cadmium in
840 the Southern Ocean: Distribution, speciation, and relation to phosphate. Limnology and
841 Oceanography **59**: 385–399. doi:10.4319/LO.2014.59.2.0385
842 Bertrand, E. M., M. A. Saito, J. M. Rose, C. R. Riesselman, M. C. Lohan, A. E. Noble, P. A.
843 Lee, and G. R. DiTullio. 2007. Vitamin B 12 and iron colimitation of phytoplankton
844 growth in the Ross Sea. Limnology and Oceanography **52**: 1079–1093.
845 doi:10.4319/lo.2007.52.3.1079
846 Biller, D. V., and K. W. Bruland. 2012. Analysis of Mn, Fe, Co, Ni, Cu, Zn, Cd, and Pb in
847 seawater using the Nobias-chelate PA1 resin and magnetic sector inductively coupled
848 plasma mass spectrometry (ICP-MS). Marine Chemistry.
849 doi:10.1016/j.marchem.2011.12.001
850 Bishop, J. K. B., and T. J. Wood. 2009. Year-round observations of carbon biomass and flux
851 variability in the Southern Ocean. Global Biogeochemical Cycles.
852 doi:10.1029/2008GB003206
853 Bown, J., P. Laan, S. Ossebaar, K. Bakker, P. Rozema, and H. J. W. de Baar. 2017. Bioactive
854 trace metal time series during Austral summer in Ryder Bay, Western Antarctic
855 Peninsula. Deep-Sea Research Part II: Topical Studies in Oceanography.
856 doi:10.1016/j.dsr2.2016.07.004
857 Boyle, E. A. 1988. Cadmium: Chemical tracer of deepwater paleoceanography.
858 Paleoceanography. doi:10.1029/PA003i004p00471
859 Boyle, E. A., F. Sclater, and J. M. Edmond. 1976. On the marine geochemistry of cadmium.
860 Nature. doi:10.1038/263042a0

https://doi.org/10.5194/egusphere-2024-2085
Preprint. Discussion started: 2 August 2024

861 Brand, L. E., W. G. Sunda, and R. R. L. Guillard. 1986. Reduction of marine phytoplankton
862 reproduction rates by copper and cadmium. Journal of Experimental Marine Biology and
863 Ecology. doi:10.1016/0022-0981(86)90205-4
864 Bruland, K. W., G. A. Knauer, and J. H. Martin. 1978. Zinc in north-east Pacific water. Nature
865 **271**: 741–743. doi:10.1038/271741a0
866 Chmiel, R. J., R. M. Kell, D. Rao, D. M. Moran, G. R. DiTullio, and M. A. Saito. 2023. Low
867 cobalt inventories in the Amundsen and Ross seas driven by high demand for labile
868 cobalt uptake among native phytoplankton communities. Biogeosciences **20**: 3997–4027.
869 doi:10.5194/bg-20-3997-2023
870 Cox, A. D., A. E. Noble, and M. A. Saito. 2014. Cadmium enriched stable isotope uptake and
871 addition experiments with natural phytoplankton assemblages in the Costa Rica
872 Upwelling Dome. Marine Chemistry. doi:10.1016/j.marchem.2014.09.009
873 Crameri, F. 2023. Scientific colour maps.doi:10.5281/ZENODO.1243862
874 Cullen, J. T. 2006. On the nonlinear relationship between dissolved cadmium and phosphate in
875 the modern global ocean: Could chronic iron limitation of phytoplankton growth cause
876 the kink? Limnology and Oceanography **51**: 1369–1380. doi:10.4319/lo.2006.51.3.1369
877 Cullen, J. T., Z. Chase, K. H. Coale, S. E. Fitzwater, and R. M. Sherrell. 2003. Effect of iron
878 limitation on the cadmium to phosphorus ratio of natural phytoplankton assemblages
879 from the Southern Ocean. Limnology and Oceanography. doi:10.4319/lo.2003.48.3.1079
880 Cullen, J. T., T. W. Lane, F. M. M. Morel, and R. M. Sheerell. 1999. Modulation of cadmium
881 uptake in phytoplankton by seawater CO2 concentration. Nature. doi:10.1038/46007

https://doi.org/10.5194/egusphere-2024-2085
Preprint. Discussion started: 2 August 2024

882 Cullen, J. T., and R. M. Sherrell. 2005. Effects of dissolved carbon dioxide, zinc, and manganese
883 on the cadmium to phosphorus ratio in natural phytoplankton assemblages. Limnology
884 and Oceanography **50**: 1193–1204. doi:10.4319/lo.2005.50.4.1193
885 Cutter, G. A., and K. W. Bruland. 2012. Rapid and noncontaminating sampling system for trace
886 elements in global ocean surveys. Limnology and Oceanography: Methods.
887 doi:10.4319/lom.2012.10.425
888 Das, P., S. Samantaray, and G. R. Rout. 1997. Studies on cadmium toxicity in plants: A review.
889 Environmental Pollution. doi:10.1016/S0269-7491(97)00110-3
890 DiTullio, G. R., N. Garcia, S. F. Riseman, and P. N. Sedwick. 2007. Effects of iron concentration
891 on pigment composition in Phaeocystis antarctica grown at low irradiance.
892 Biogeochemistry **83**: 71–81. doi:10.1007/s10533-007-9080-8
893 DiTullio, G. R., M. E. Geesey, A. Leventer, and M. P. Lizotte. 2003. Algal pigment ratios in the
894 Ross Sea: Implications for Chemtax analysis of Southern Ocean data, p. 35–51. *In*.
895 DiTullio, G. R., and W. O. Smith. 1995. Relationship between dimethylsulfide and
896 phytoplankton pigment concentrations in the Ross Sea, Antarctica. Deep-Sea Research
897 Part I. doi:10.1016/0967-0637(95)00051-7
898 Ellwood, M. J. 2008. Wintertime trace metal (Zn, Cu, Ni, Cd, Pb and Co) and nutrient
899 distributions in the Subantarctic Zone between 40-52°S; 155-160°E. Marine Chemistry.
900 doi:10.1016/j.marchem.2008.07.008
901 Ellwood, M. J., and K. A. Hunter. 2000. The incorporation of zinc and iron into the frustule of
902 the marine diatom Thalassiosira pseudonana. Limnology and Oceanography.
903 doi:10.4319/lo.2000.45.7.1517

https://doi.org/10.5194/egusphere-2024-2085
Preprint. Discussion started: 2 August 2024

904 Fitzwater, S. E., K. S. Johnson, R. M. Gordon, K. H. Coale, and W. O. Smith. 2000. Trace metal
905 concentrations in the Ross Sea and their relationship with nutrients and phytoplankton
906 growth. Deep-Sea Research Part II: Topical Studies in Oceanography **47**: 3159–3179.
907 doi:10.1016/S0967-0645(00)00063-1
908 Gerringa, L. J. A., A.-C. Alderkamp, G. van Dijken, P. Laan, R. Middag, and K. R. Arrigo. 2020.
909 Dissolved Trace Metals in the Ross Sea. Frontiers in Marine Science **7**.
910 doi:10.3389/fmars.2020.577098
911 Giordano, R., G. Lombardi, L. Ciaralli, E. Beccaloni, A. Sepe, M. Ciprotti, and S. Costantini.
912 1999. Major and trace elements in sediments from Terra Nova Bay, Antarctica. Science
913 of The Total Environment **227**: 29–40. doi:10.1016/S0048-9697(98)00402-1
914 Haas, C. E., D. A. Rodionov, J. Kropat, D. Malasarn, S. S. Merchant, and V. de Crécy-Lagard.
915 2009. A subset of the diverse COG0523 family of putative metal chaperones is linked to
916 zinc homeostasis in all kingdoms of life. BMC Genomics **10**: 470. doi:10.1186/1471-
917 2164-10-470
918 Hopwood, M. J., D. Carroll, J. Höfer, and others. 2019. Highly variable iron content modulates
919 iceberg-ocean fertilisation and potential carbon export. Nature Communications 2019
920 10:1 **10**: 1–10. doi:10.1038/s41467-019-13231-0
921 Horner, T. J., R. B. Y. Lee, G. M. Henderson, and R. E. M. Rickaby. 2013. Nonspecific uptake
922 and homeostasis drive the oceanic cadmium cycle. Proceedings of the National Academy
923 of Sciences **110**: 2500–2505. doi:10.1073/pnas.1213857110
924 Horner, T. J., S. H. Little, T. M. Conway, and others. 2021. Bioactive Trace Metals and Their
925 Isotopes as Paleoproductivity Proxies: An Assessment Using GEOTRACES-Era Data.
926 Global Biogeochemical Cycles **35**: e2020GB006814. doi:10.1029/2020GB006814

https://doi.org/10.5194/egusphere-2024-2085
Preprint. Discussion started: 2 August 2024

927 Hutchins, D. A., and K. W. Bruland. 1995. Fe, Zn, Mn and N transfer between size classes in a
928 coastal phytoplankton community: Trace metal and major nutrient recycling compared.
929 issn: 0022-2402 **53**: 297–313. doi:10.1357/0022240953213197
930 Hutchins, D. A., W. X. Wang, M. A. Schmidt, and N. S. Fisher. 1999. Dual-labeling techniques
931 for trace metal biogeochemical investigations in aquatic plankton communities. Aquatic
932 Microbial Ecology. doi:10.3354/ame019129
933 Hutchins, D., and K. Bruland. 1994. Grazer-mediated regeneration and assimilation of Fe, Zn
934 and Mn from planktonic prey. Mar. Ecol. Prog. Ser. **110**: 259–269.
935 doi:10.3354/meps110259
936 Irving, B. H., and R. J. P. Williams. 1953. The Stability of Transition-metal Complexes. Journal
937 of the Chemical Society (Resumed). doi:10.1039/JR9530003192
938 Jackson, S. L., J. Spence, D. J. Janssen, A. R. S. Ross, and J. T. Cullen. 2018. Determination of
939 Mn, Fe, Ni, Cu, Zn, Cd and Pb in seawater using offline extraction and triple quadrupole
940 ICP-MS/MS. Journal of Analytical Atomic Spectrometry **33**: 304–313.
941 doi:10.1039/c7ja00237h
942 Kell, R. M., A. V. Subhas, N. L. Schanke, and others. 2023. Zinc stimulation of phytoplankton in
943 a low carbon dioxide, coastal Antarctic environment.doi:10.1101/2023.11.05.565706
944 Kellogg, R. M., M. A. Moosburner, N. R. Cohen, and others. 2022. Adaptive responses of
945 marine diatoms to zinc scarcity and ecological implications. Nature Communications
946 2022 13:1 **13**: 1–13. doi:10.1038/s41467-022-29603-y
947 Lane, E. S., D. M. Semeniuk, R. F. Strzepek, J. T. Cullen, and M. T. Maldonado. 2009. Effects
948 of iron limitation on intracellular cadmium of cultured phytoplankton: Implications for

https://doi.org/10.5194/egusphere-2024-2085
Preprint. Discussion started: 2 August 2024

surface dissolved cadmium to phosphate ratios. Marine Chemistry **115**: 155–162. doi:10.1016/J.MARCHEM.2009.07.008

Lane, T. W., M. A. Saito, G. N. George, I. J. Pickering, R. C. Prince, and F. M. M. Morel. 2005. A cadmium enzyme from a marine diatom. Nature **435**: 42–42. doi:10.1038/435042a

Latour, P., K. Wuttig, P. van der Merwe, and others. 2021. Manganese biogeochemistry in the Southern Ocean, from Tasmania to Antarctica. Limnology and Oceanography **66**: 2547–2562. doi:10.1002/lno.11772

Lee, J. G., S. B. Roberts, and F. M. M. Morel. 1995. Cadmium: A nutrient for the marine diatom Thalassiosira weissflogii. Limnology and Oceanography. doi:10.4319/lo.1995.40.6.1056

Lee, J., and F. Morel. 1995. Replacement of zinc by cadmium in marine phytoplankton. Marine Ecology Progress Series **127**: 305–309. doi:10.3354/meps127305

Lohan, M. C., P. J. Statham, and D. W. Crawford. 2002. Total dissolved zinc in the upper water column of the subarctic North East Pacific. Deep Sea Research Part II: Topical Studies in Oceanography **49**: 5793–5808. doi:10.1016/S0967-0645(02)00215-1

Martin, J. H. 1990. Glacial-interglacial CO2 change: The Iron Hypothesis. Paleoceanography. doi:10.1029/PA005i001p00001

Middag, R., H. J. W. Baar, and K. W. Bruland. 2019. The relationships netween dissolved zinc and major nutrients phosphate and silicate along the GEOTRACES GA02 transect in the West Atlantic Ocean. Global Biogeochemical Cycles **33**: 63–84. doi:10.1029/2018GB006034

Morel, F. M. M., P. J. Lam, and M. A. Saito. 2020. Trace metal substitution in marine phytoplankton. Annual Review of Earth and Planetary Sciences **48**: 491–517. doi:10.1146/annurev-earth-053018-060108

https://doi.org/10.5194/egusphere-2024-2085
Preprint. Discussion started: 2 August 2024

Morel, F. M. M., A. J. Milligan, and M. A. Saito. 2013. Marine Bioinorganic Chemistry: The Role of Trace Metals in the Oceanic Cycles of Major Nutrients, *In* Treatise on Geochemistry: Second Edition.

Morel, F. M. M., J. R. Reinfelder, S. B. Roberts, C. P. Chamberlain, J. G. Lee, and D. Yee. 1994. Zinc and carbon co-limitation of marine phytoplankton. Nature **369**: 740–742. doi:10.1038/369740A0

Noble, A. E., C. H. Lamborg, D. C. Ohnemus, and others. 2012. Basin-scale inputs of cobalt, iron, and manganese from the Benguela-Angola front to the South Atlantic Ocean. Limnology and Oceanography. doi:10.4319/lo.2012.57.4.0989

Noble, A. E., D. M. Moran, A. E. Allen, and M. A. Saito. 2013. Dissolved and particulate trace metal micronutrients under the McMurdo Sound seasonal sea ice: basal sea ice communities as a capacitor for iron. Frontiers in Chemistry **1**. doi:10.3389/fchem.2013.00025

Ohnemus, D. C., S. Rauschenberg, G. A. Cutter, J. N. Fitzsimmons, R. M. Sherrell, and B. S. Twining. 2017. Elevated trace metal content of prokaryotic communities associated with marine oxygen deficient zones. Limnology and Oceanography. doi:10.1002/lno.10363

Oldham, V. E., R. Chmiel, C. M. Hansel, G. R. DiTullio, D. Rao, and M. Saito. 2021. Inhibited Manganese Oxide Formation Hinders Cobalt Scavenging in the Ross Sea. Global Biogeochemical Cycles **35**. doi:10.1029/2020GB006706

Park, H., P. J. McGinn, and F. M. M. Morel. 2008. Expression of cadmium carbonic anhydrase of diatoms in seawater. Aquatic Microbial Ecology. doi:10.3354/ame01192

https://doi.org/10.5194/egusphere-2024-2085
Preprint. Discussion started: 2 August 2024

993 Park, H., B. Song, and F. M. M. Morel. 2007. Diversity of the cadmium-containing carbonic
994 anhydrase in marine diatoms and natural waters. Environmental Microbiology.
995 doi:10.1111/j.1462-2920.2006.01151.x
996 Person, R., M. Vancoppenolle, O. Aumont, and M. Malsang. 2021. Continental and Sea Ice Iron
997 Sources Fertilize the Southern Ocean in Synergy. Geophysical Research Letters **48**:
998 e2021GL094761. doi:10.1029/2021GL094761
999 Price, N. M., and F. M. M. Morel. 1990. Cadmium and cobalt substitution for zinc in a marine
1000 diatom. Nature **344**: 658–660. doi:10.1038/344658a0
1001 Rapp, I., C. Schlosser, D. Rusiecka, M. Gledhill, and E. P. Achterberg. 2017. Automated
1002 preconcentration of Fe, Zn, Cu, Ni, Cd, Pb, Co, and Mn in seawater with analysis using
1003 high-resolution sector field inductively-coupled plasma mass spectrometry. Analytica
1004 Chimica Acta. doi:10.1016/j.aca.2017.05.008
1005 Roshan, S., T. DeVries, J. Wu, and G. Chen. 2018. The Internal Cycling of Zinc in the Ocean.
1006 Global Biogeochemical Cycles **32**: 1833–1849. doi:10.1029/2018GB006045
1007 Rudge, J. F., B. C. Reynolds, and B. Bourdon. 2009. The double spike toolbox. Chemical
1008 Geology. doi:10.1016/j.chemgeo.2009.05.010
1009 Saito, M. A., and T. J. Goepfert. 2008. Zinc-cobalt colimitation of *Phaeocystis antarctica*.
1010 Limnology and Oceanography **53**: 266–275. doi:10.4319/lo.2008.53.1.0266
1011 Sedwick, P. N., G. R. Di Tullio, and D. J. Mackey. 2000. Iron and manganese in the Ross Sea,
1012 Seasonal iron limitation in Antarctic. Journal of Geophysical Research: Oceans.
1013 doi:10.1029/2000JC000256
1014 Sedwick, P. N., C. M. Marsay, B. M. Sohst, and others. 2011. Early season depletion of
1015 dissolved iron in the Ross Sea polynya: Implications for iron dynamics on the Antarctic

https://doi.org/10.5194/egusphere-2024-2085
Preprint. Discussion started: 2 August 2024

continental shelf. Journal of Geophysical Research **116**: C12019. doi:10.1029/2010JC006553

Shaked, Y., Y. Xu, K. Leblanc, and F. M. M. Morel. 2006. Zinc availability and alkaline phosphatase activity in Emiliania huxleyi: Implications for Zn-P co-limitation in the ocean. Limnology and Oceanography **51**: 299–309. doi:10.4319/lo.2006.51.1.0299

Sieber, M., T. M. Conway, G. F. de Souza, C. S. Hassler, M. J. Ellwood, and D. Vance. 2020. Cycling of zinc and its isotopes across multiple zones of the Southern Ocean: Insights from the Antarctic Circumnavigation Expedition. Geochimica et Cosmochimica Acta. doi:10.1016/j.gca.2019.09.039

Sohrin, Y., S. Urushihara, S. Nakatsuka, T. Kono, E. Higo, T. Minami, K. Norisuye, and S. Umetani. 2008. Multielemental determination of GEOTRACES key trace metals in seawater by ICPMS after preconcentration using an ethylenediaminetriacetic acid chelating resin. Analytical Chemistry. doi:10.1021/ac800500f

de Souza, G. F., S. P. Khatiwala, M. P. Hain, S. H. Little, and D. Vance. 2018. On the origin of the marine zinc–silicon correlation. Earth and Planetary Science Letters **492**: 22–34. doi:10.1016/j.epsl.2018.03.050

St-Laurent, P., P. L. Yager, R. M. Sherrell, S. E. Stammerjohn, and M. S. Dinniman. 2017. Pathways and supply of dissolved iron in the Amundsen Sea (Antarctica). Journal of Geophysical Research: Oceans **122**: 7135–7162. doi:10.1002/2017JC013162

Sunda, W. G., and S. A. Huntsman. 1992. Feedback interactions between zinc and phytoplankton in seawater. Limnology and Oceanography **37**: 25–40. doi:10.4319/lo.1992.37.1.0025

https://doi.org/10.5194/egusphere-2024-2085
Preprint. Discussion started: 2 August 2024

1037 Sunda, W. G., and S. A. Huntsman. 1995. Cobalt and zinc interreplacement in marine
1038 phytoplankton: Biological and geochemical implications. Limnology and Oceanography
1039 **40**: 1404–1417. doi:10.4319/lo.1995.40.8.1404
1040 Sunda, W. G., and S. A. Huntsman. 1996. Antagonisms between cadmium and zinc toxicity and
1041 manganese limitation in a coastal diatom. Limnology and Oceanography **41**: 373–387.
1042 doi:10.4319/lo.1996.41.3.0373
1043 Sunda, W. G., and S. A. Huntsman. 1998a. Processes regulating cellular metal accumulation and
1044 physiological effects: Phytoplankton as model systems. Science of The Total
1045 Environment **219**: 165–181. doi:10.1016/S0048-9697(98)00226-5
1046 Sunda, W. G., and S. A. Huntsman. 1998b. Control of Cd Concentrations in a Coastal Diatom by
1047 Interactions among Free Ionic Cd, Zn, and Mn in Seawater. Environmental Science &
1048 Technology **32**: 2961–2968. doi:10.1021/es980271y
1049 Sunda, W. G., and S. A. Huntsman. 2000. Effect of Zn, Mn, and Fe on Cd accumulation in
1050 phytoplankton: Implications for oceanic Cd cycling. Limnology and Oceanography **45**:
1051 1501–1516. doi:10.4319/lo.2000.45.7.1501
1052 Tan, D., W. Xu, Z. Zhu, S. Li, G. Wu, and H. Qin. 2020. Optimizing the ratio of the spike to
1053 sample for isotope dilution analysis: a case study with selenium isotopes. Acta
1054 Geochimica. doi:10.1007/s11631-019-00390-6
1055 Twining, B. S., and S. B. Baines. 2013. The trace metal composition of marine phytoplankton.
1056 Annual review of marine science **5**: 191–215. doi:10.1146/annurev-marine-121211-
1057 172322

https://doi.org/10.5194/egusphere-2024-2085
Preprint. Discussion started: 2 August 2024

1058 Twining, B. S., S. B. Baines, and N. S. Fisher. 2004. Element stoichiometries of individual
1059 plankton cells collected during the Southern Ocean Iron Experiment (SOFeX).
1060 Limnology and Oceanography **49**: 2115–2128. doi:10.4319/LO.2004.49.6.2115
1061 Twining, B. S., S. D. Nodder, A. L. King, and others. 2014. Differential remineralization of
1062 major and trace elements in sinking diatoms. Limnology and Oceanography **59**: 689–704.
1063 doi:10.4319/LO.2014.59.3.0689
1064 Vance, D., S. H. Little, G. F. De Souza, S. Khatiwala, M. C. Lohan, and R. Middag. 2017.
1065 Silicon and zinc biogeochemical cycles coupled through the Southern Ocean. Nature
1066 Geoscience **10**: 202–206. doi:10.1038/NGEO2890
1067 Weber, T., S. John, A. Tagliabue, and T. DeVries. 2018. Biological uptake and reversible
1068 scavenging of zinc in the global ocean. Science **361**: 72–76.
1069 doi:10.1126/SCIENCE.AAP8532
1070 Wright, S. W., R. L. van den Enden, I. Pearce, A. T. Davidson, F. J. Scott, and K. J. Westwood.
1071 2010. Phytoplankton community structure and stocks in the Southern Ocean (30-80°E)
1072 determined by CHEMTAX analysis of HPLC pigment signatures. Deep-Sea Research
1073 Part II: Topical Studies in Oceanography. doi:10.1016/j.dsr2.2009.06.015
1074 Wu, J., and E. A. Boyle. 1998. Determination of iron in seawater by high-resolution isotope
1075 dilution inductively coupled plasma mass spectrometry after Mg(OH)2 coprecipitation.
1076 Analytica Chimica Acta **367**: 183–191. doi:10.1016/S0003-2670(98)00145-7
1077 Wuttig, K., A. T. Townsend, P. van der Merwe, and others. 2019. Critical evaluation of a
1078 seaFAST system for the analysis of trace metals in marine samples. Talanta.
1079 doi:10.1016/j.talanta.2019.01.047

https://doi.org/10.5194/egusphere-2024-2085
Preprint. Discussion started: 2 August 2024

1080 Xu, Y., D. Tang, Y. Shaked, and F. M. M. Morel. 2007. Zinc, cadmium, and cobalt
1081 interreplacement and relative use efficiencies in the coccolithophore Emiliania huxleyi.
1082 Limnology and Oceanography **52**: 2294–2305. doi:10.4319/lo.2007.52.5.2294
1083 Zhao, Y., D. Vance, W. Abouchami, and H. J. W. de Baar. 2014. Biogeochemical cycling of zinc
1084 and its isotopes in the Southern Ocean. Geochimica et Cosmochimica Acta.
1085 doi:10.1016/j.gca.2013.07.045
1086